

M. Eiber, A. Baskin, M. Essler, K. Holzapfel,
O. Ratib, K. Scheidbauer, and J.-P. Willi

Contents

Lymphoma, Lung and Other Tumors	169
Diffuse Large B-Cell Lymphoma.....	170
Recurrence of Chondrosarcoma.....	172
Metastatic Pulmonary Cancer (NSCLC).....	174
Esophageal Cancer with Liver Metastases	176
Multi-Focal Lung Tumor.....	178
Brain Metastasis of Unknown Origin	180
Pulmonary Adenocarcinoma	182
PET/MR in Acute Lymphocytic Leukemia (ALL)	184
PET/MR for Biopsy Planning in NHL with Bone Infiltration	186
Recurrent T-NHL with Bone Infiltration.....	188
Liver Metastasis of Adenocarcinoma of the Adrenal Gland.....	190
Liver Metastases of Colorectal Cancer	192
Liver Metastasis of Rectal Cancer.....	194
References	196

Lymphoma, Lung and Other Tumors

In both Hodgkin disease and non-Hodgkin lymphoma, imaging plays an important role for primary diagnosis and staging [1]. Except for cerebral lymphoma, whole-body MRI is of high research interest but not clinical routine in the staging algorithm of lymphoma patients. This situation could change quickly, and whole-body MRI might become a good alternative to CT [2]. Especially when combining with whole-body diffusion-weighted MRI, with its high sensitivity could improve the diagnostic accuracy for the staging of Hodgkin disease and non-Hodgkin lymphoma [3, 4]. Alternatively, combining MR and ¹⁸F-FDG PET might further increase diagnostic accuracy and play an important role as research tool in evaluating the strengths and draw-backs of both modalities directly against each other. This might also give additional data on the view of some authors who argue that ¹⁸F-FDG PET/CT might even eliminate the need for bone marrow biopsy in the primary staging of Hodgkin disease because ¹⁸F-FDG PET/CT is highly sensitive and specific for bone marrow involvement in this disease, at 92 % and 90 % respectively [5]. Additional information using PET/MR could be specifically gained from diffusion-weighted sequences in the case of indolent lymphomas [6]. Finally due the lack of radiation exposure of MRI, compared with CT, PET/MRI may get an alternative to PET/CT especially in young patients with good prognosis.

MR in general is considered to be inferior to CT for staging of lung cancer and detection of pulmonary metastases [7, 8]. However MRI, including DWI sequences, has been shown to detect 100 % of lung metastases larger than 7 mm found on CT and the presence of small metastases is often not therapeutically relevant [9, 10]. Hereby first preliminary data indicate an equivalent accuracy of PET/MR and PET/CT for lung lesions [11]. In addition, new developments like half-Fourier, single-shot, turbo spin echo sequences have substantially improved the lung-tissue contrast of MRI in the recent years [8]. With regard to local tumor infiltration into adjacent structures MRI might improve T-staging when compared to CT.

M. Eiber (✉) • K. Holzapfel
Department of Radiology,
Technische Universität München,
Munich, Germany
e-mail: matthias.eiber@tum.de

A. Baskin • O. Ratib • J.-P. Willi
Department of Medical Imaging,
Division of Nuclear Medicine and Molecular Imaging,
Geneva University and Geneva University Hospitals,
Geneva, Switzerland

M. Essler • K. Scheidbauer
Department of Nuclear Medicine,
Technische Universität München,
Munich, Germany

Diffuse Large B-Cell Lymphoma

Clinical History

Thirty-eight-year-old patient with diffuse large B-cell lymphoma (originally as gastric MALT). Follow-up study acquired after two cycles of chemotherapy. Status post renal transplant at age of 19.

Imaging Technique

PET: Whole-body PET acquired 60 min after injection of 369 MBq of ^{18}F -FDG, 57 kg/157 cm patient, with 5.2 mmol/L of fasting glycemia.

MRI: Whole body atMR (T1 weighted), supine position. 3D FFE T1 weighted (eThrive) whole-body MRI.

Findings

Initial staging study prior to treatment showed multiple hypermetabolic lymph nodes in the coeliac and retroperitoneal areas. Super diaphragmatic extension showed a single positive supraclavicular lymph node. Follow-up study after two cycles of chemotherapy show complete normalization of lymph nodes metabolic activity.

Teaching Points

Although whole-body MR images may not provide similar diagnostic anatomical resolution as PET/CT, PET/MR may be a valuable alternative technique for assessment of the extent of the disease and response to chemotherapy particularly in patients with limited renal function that may be at risk of renal toxicity from CT contrast media.

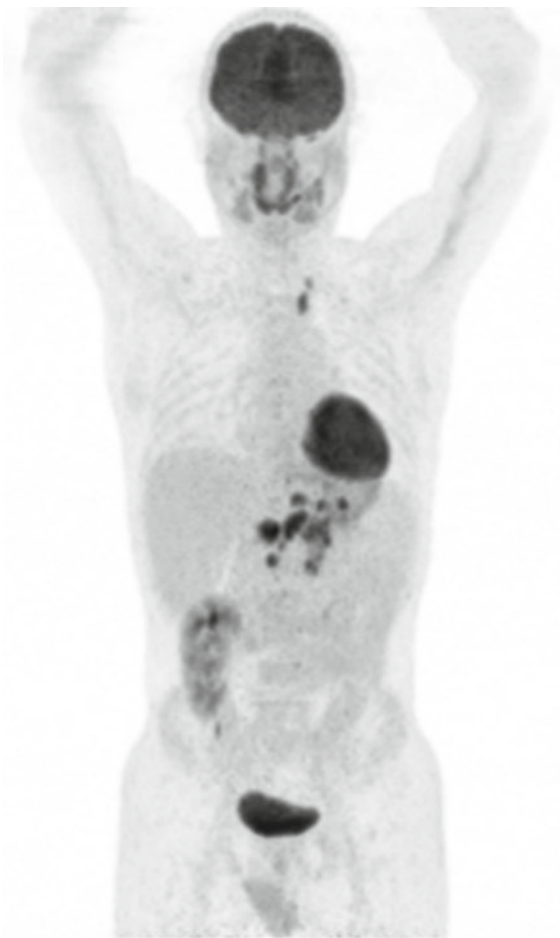


Fig. 10.1 Coronal MIP reconstruction of PET images acquired at the time of the diagnosis showing diffuse hyper-metabolic lymph nodes in the coeliac and retroperitoneal area and in the upper left clavicular area



Fig. 10.2 Whole body coronal MR and PET images showing complete resolution of the hyper metabolic lymph nodes 2 month later after two cycles of chemotherapy

Fig. 10.3 Comparison of coronal PET/CT (*top*) and PET/MR (*bottom*) images acquired after chemotherapy showing complete resolution of abdominal and thoracic metabolic lymph nodes. Note the medullar hyper-metabolism post chemotherapy

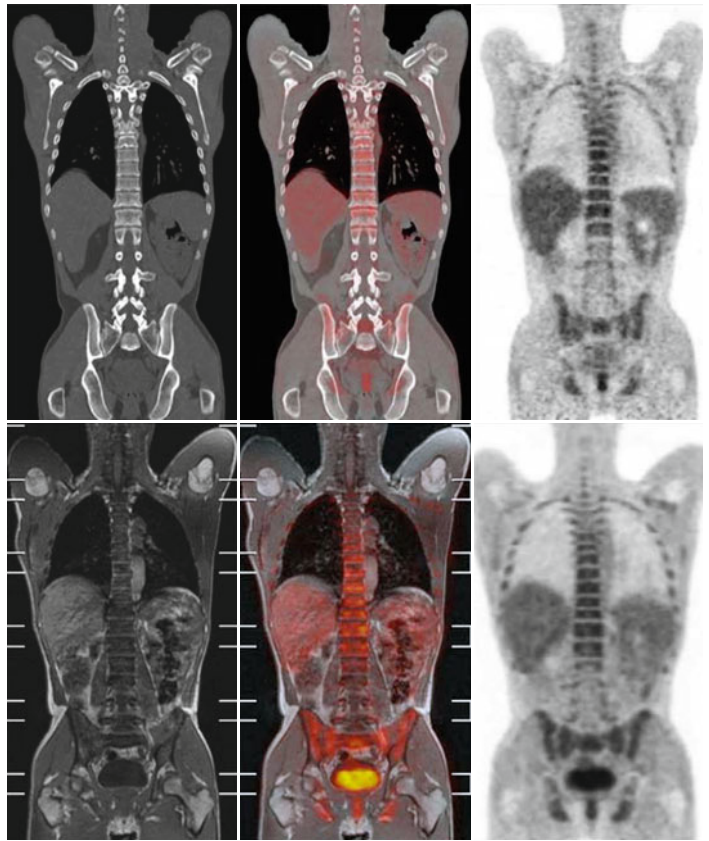
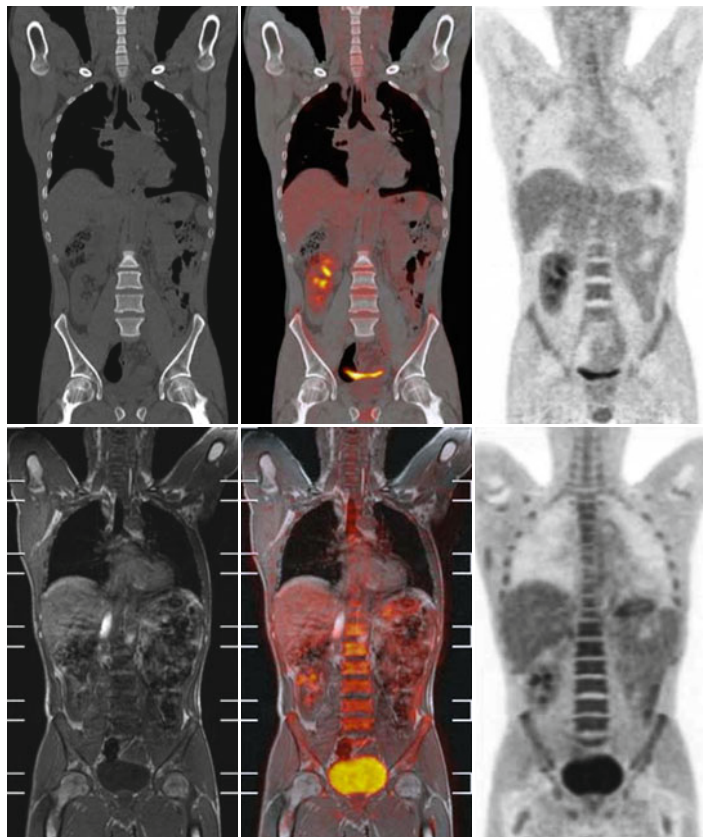


Fig. 10.4 Coronal images of PET/CT (*top*) and PET/MR (*bottom*) studies located more posteriorly. Notice the right transplanted kidney



Recurrence of Chondrosarcoma

Clinical History

Thirty-five-year-old patient with a history of surgical removal of a mixoide chondrosarcoma of the left thigh followed by radio- and chemo-therapy 2 years ago. Current study requested for investigation of recurrence of extra-articular multi-metastatic extension of the original tumor.

Imaging Technique

PET: Whole-body PET acquired 60 min after injection of 369 MBq of ^{18}F -FDG, 57 kg/157 cm patient, with 5.2 mmol/L of fasting glycemia.

MRI: Whole body atMR (T1 weighted), supine position followed by a whole body 3D FFE T1 weighted (eThrive) MRI.

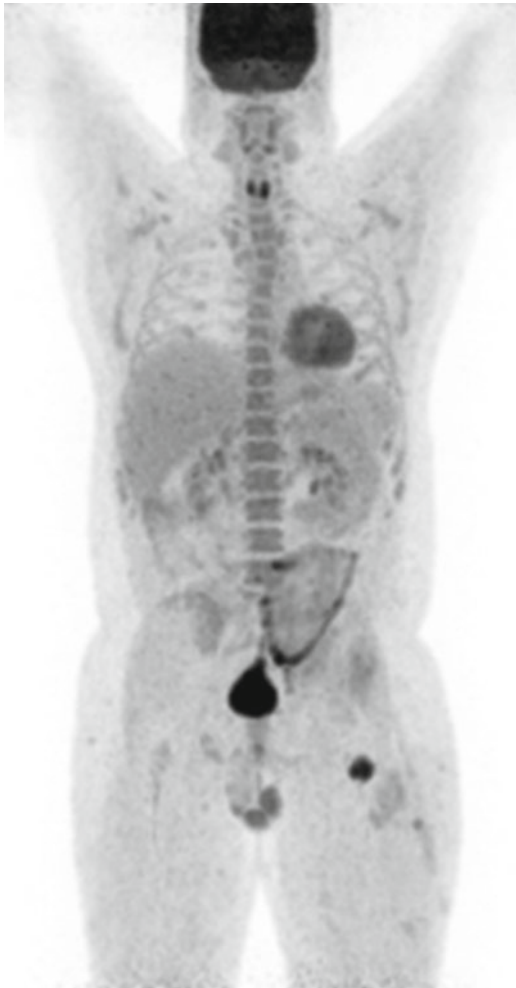


Fig. 10.5 Whole body volume MIP rendering of PET images showing focal uptake in the tumor region of the left thigh and distant focal uptake lesions in the abdomen

Findings

Current study shows recurrence of soft tissue lesion of the left thigh with focal increase in FDG uptake with remote metastatic extension of hepermetabolic lesions in the iliac and peritoneal area of the left abdomen and pelvic area.

Teaching Points

For soft tissue tumors, high-resolution MR images can provide more adequate soft tissue differentiation and anatomical localization than CT images

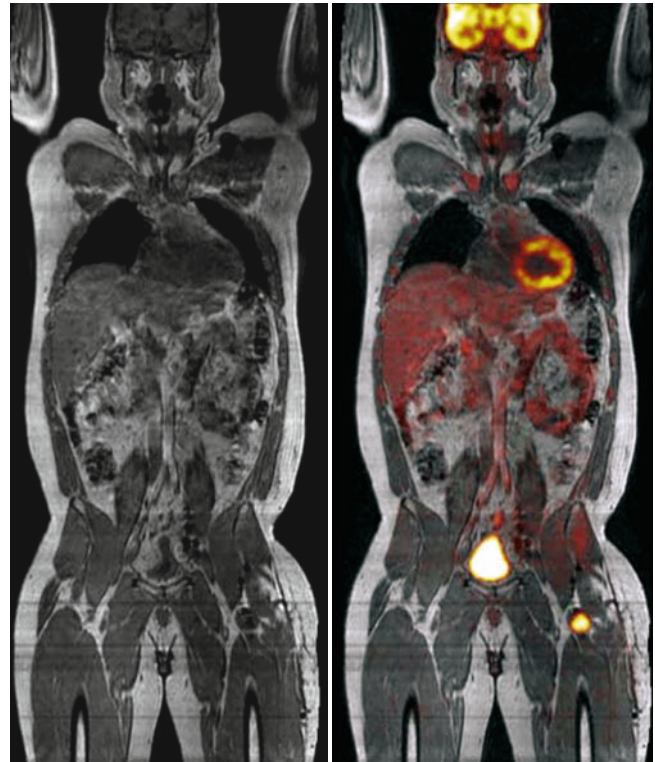


Fig. 10.6 Coronal MPR of whole-body eThrive MRI images (*left*) and fusion with PET images (*right*)

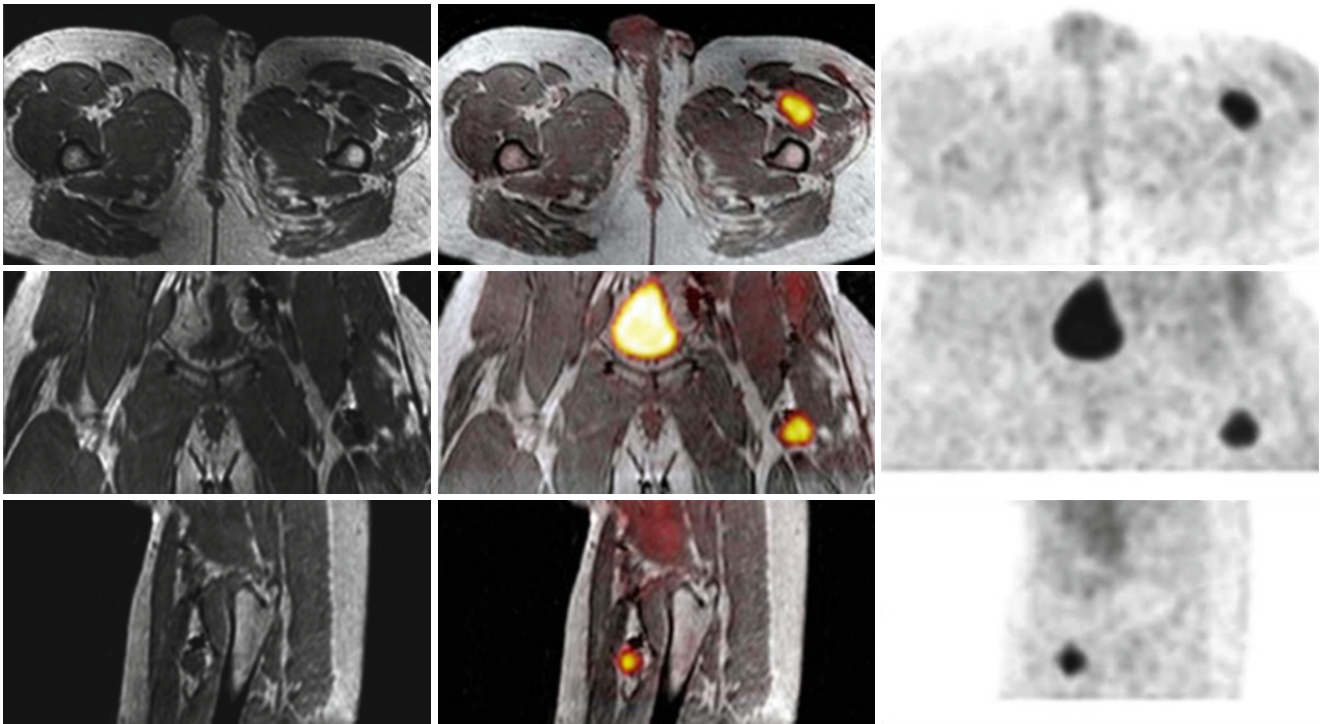


Fig. 10.7 Multi-planar reformatted (MPR) images of high resolution TSE T2 weighted (eThrive) MRI images fused with PET images at the level of the muscular lesion in the left thigh

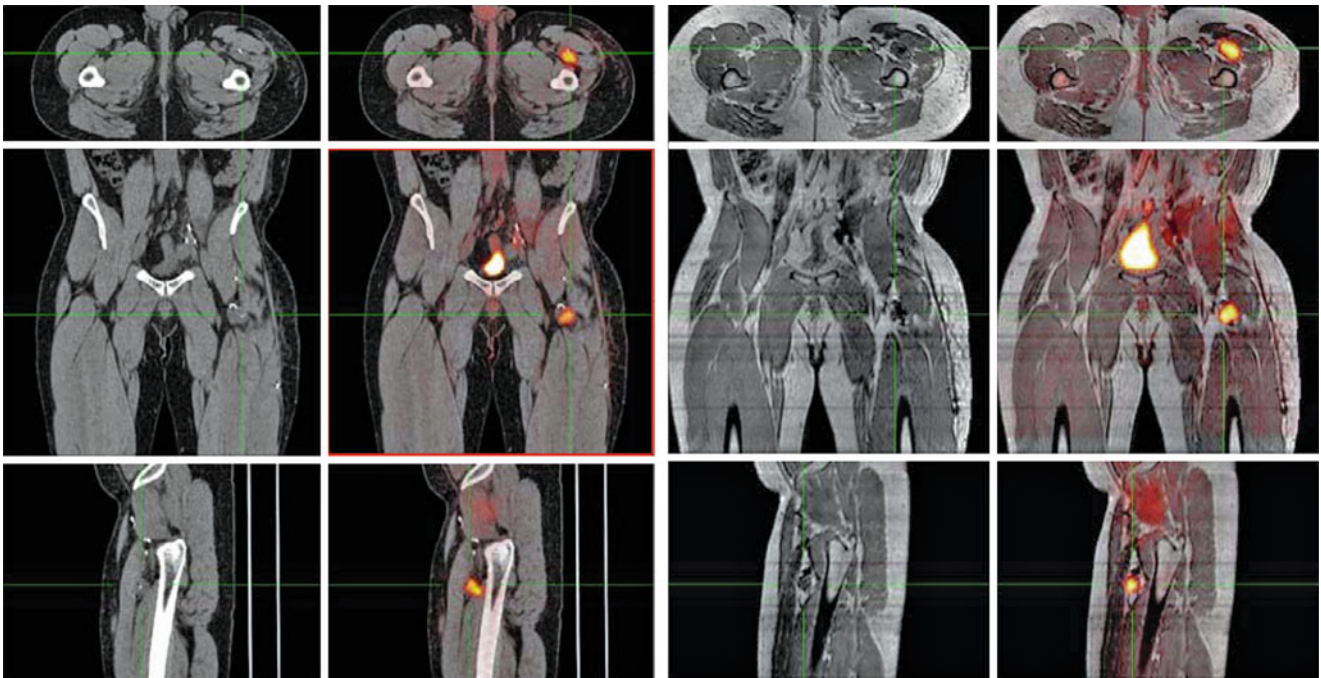


Fig. 10.8 Comparison of PET/CT (*left*) and PET/MR (*right*) multi-planar (MPR) reformatted images of the pelvis and mid thigh region obtained from whole-body 3D images

Metastatic Pulmonary Cancer (NSCLC)

Clinical History

Seventy-year-old patient diagnosed with non-small cell lung cancer (NSCLC) with liver metastases. Follow-up study requested 3 months after chemotherapy.

Imaging Technique

PET: Whole-body PET acquired 60 min after injection of 370 MBq of ^{18}F -FDG.

MRI: Whole body atMR (T1 weighted), supine position. 3D FFE T1 weighted (eThrive) MRI followed by coronal high-resolution breath-hold HASTE images of the upper abdomen.

Findings

PET/MR shows left lower lobe lung cancer with metastatic mediastinal lymph node and heterogeneous tracer uptake in large lesion (7 × 9 cm) in right liver segments VI/VII corresponding to metastatic disease.

Teaching Points

For liver metastases, high-resolution breath-hold MR images can provide better definition and tissue characterization than contrast-enhanced CT images.



Fig. 10.9 Coronal view of volume rendered MIP of PET images showing focal FDG uptake in the left para-hilar region and a large metastatic lesion of the liver with central hypometabolism corresponding to necrotic tissue

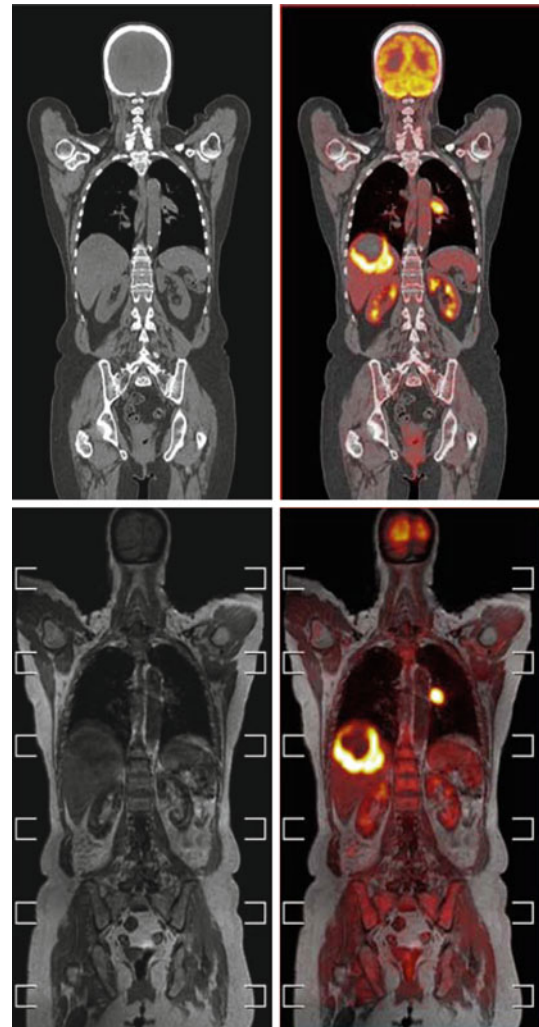


Fig. 10.10 Comparison of coronal views of whole body PET/CT (*top*) and low resolution whole-body PET/MR (*bottom*)

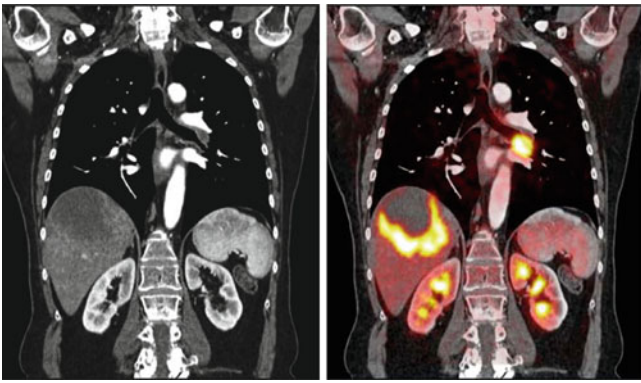


Fig. 10.11 High-resolution contrast-enhanced CT (*left*) and fusion (*right*) of PET/CT images of the thorax and upper abdomen

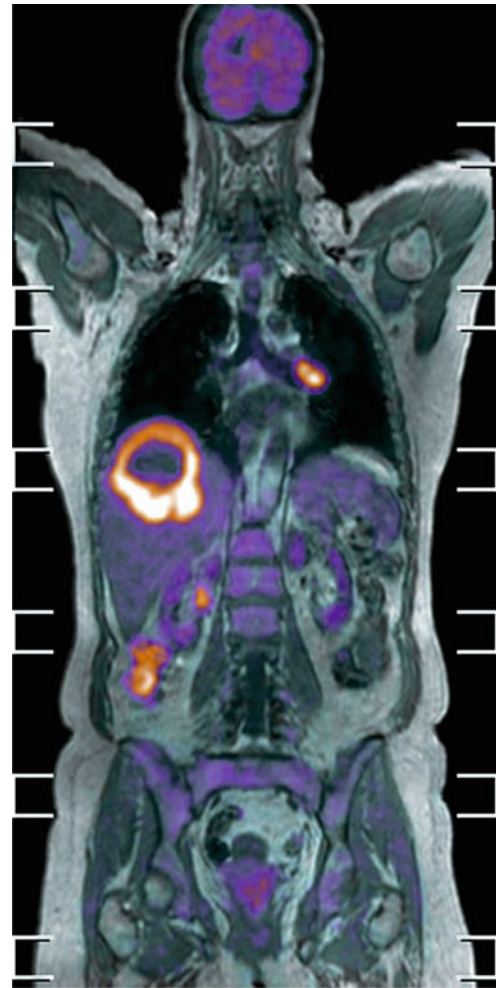


Fig. 10.12 Coronal view of low-resolution whole-body MR fused with corresponding PET image

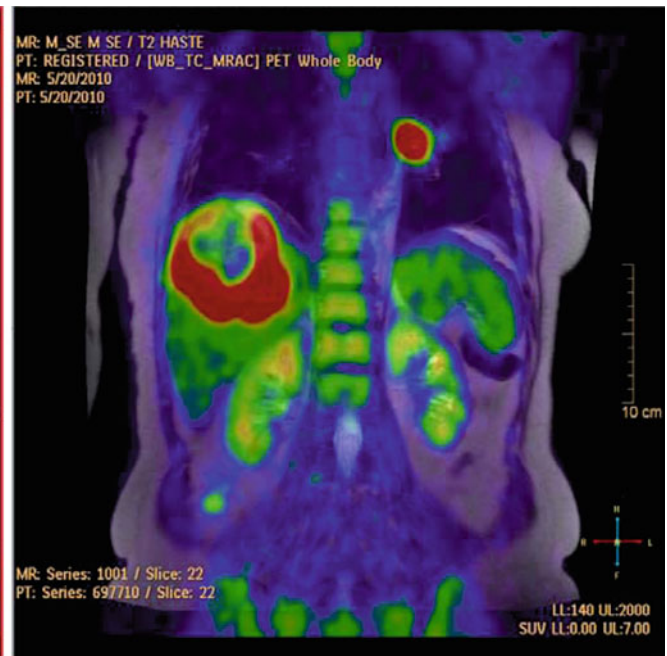
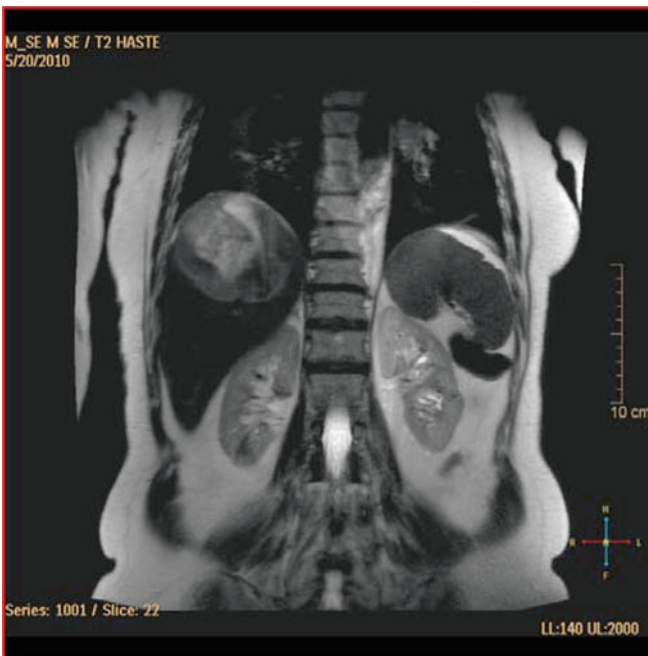


Fig. 10.13 High-resolution breath-hold coronal HASTE MR image (*left*) with corresponding PET/MR image (*right*)

Esophageal Cancer with Liver Metastases

Clinical History

Sixty-year-old patient investigated for staging of a distal esophageal adenocarcinoma of the oeso-gastric junction. Status post chemotherapy.

Imaging Technique

PET: Whole-body PET acquired 60 min after injection of 370 MBq of ^{18}F -FDG.

MRI: Whole body atMR (T1 weighted), supine position. Followed by a complementary diagnostic MRI study acquired on a Siemens Espree including a T2 HASTE MRI sequences in coronal. 3D FFE T1 weighted (eThrive) sequence with contrast injection.

Findings

PET/MR shows the hypermetabolic tumor lesion of the oeso-gastric junction, and a focal metastatic lesion of the liver with high FDG uptake. Incidental finding of a benign hepatic lesion without tracer uptake, most likely an hemangioma.

Teaching Points

Combination of diagnostic MR sequences and PET images allow to better differentiate malignant from benign lesions of the liver.



Fig. 10.14 Coronal view of volume rendered MIP of PET images showing two focal lesions of FDG uptake in the oeso-gastric junction (red arrow) and in a liver metastasis (yellow arrow)

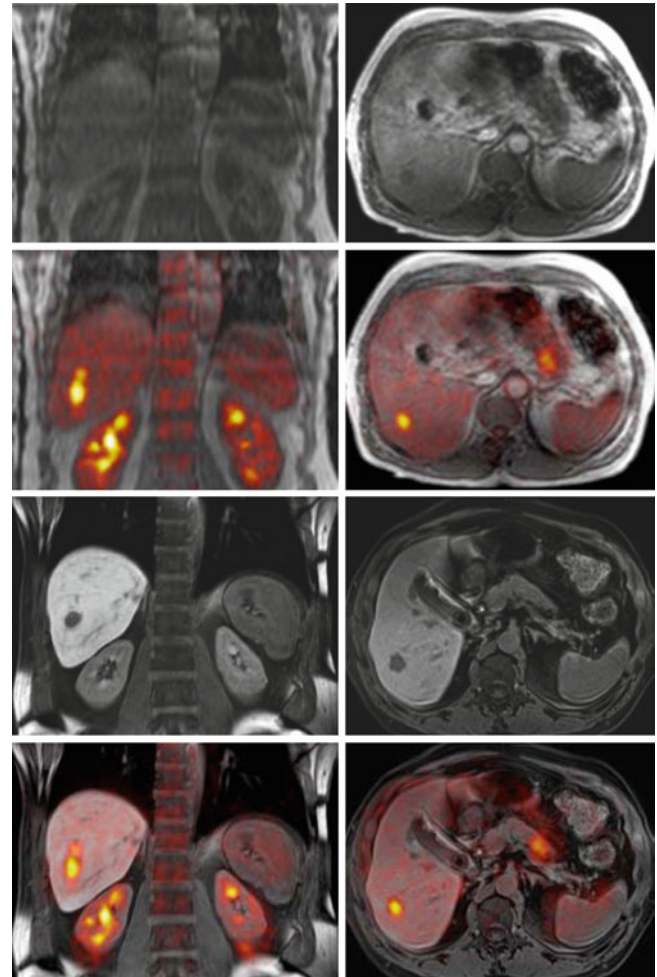


Fig. 10.15 Comparison of low-resolution whole-body MRI images (top) and high resolution (T1 weighted VIBE) MR sequences (bottom) fused with corresponding PET images

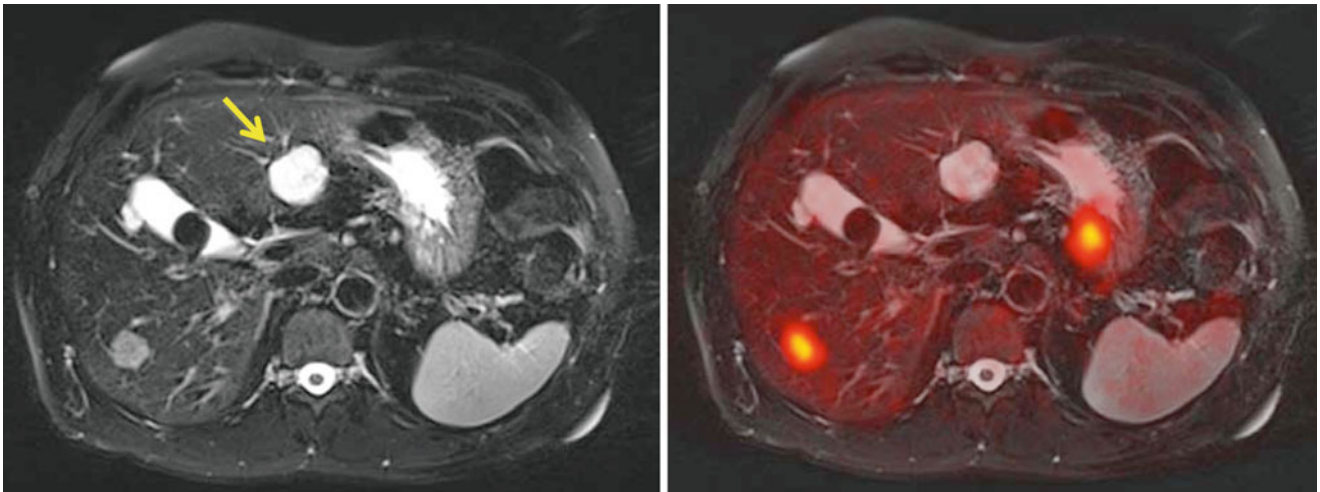


Fig. 10.16 High-resolution 2D fat-saturated “BLADE” MR images (*left*) fused with corresponding PET image (*right*) showing a benign lesion (*arrow*) with absence of FDG uptake on PET

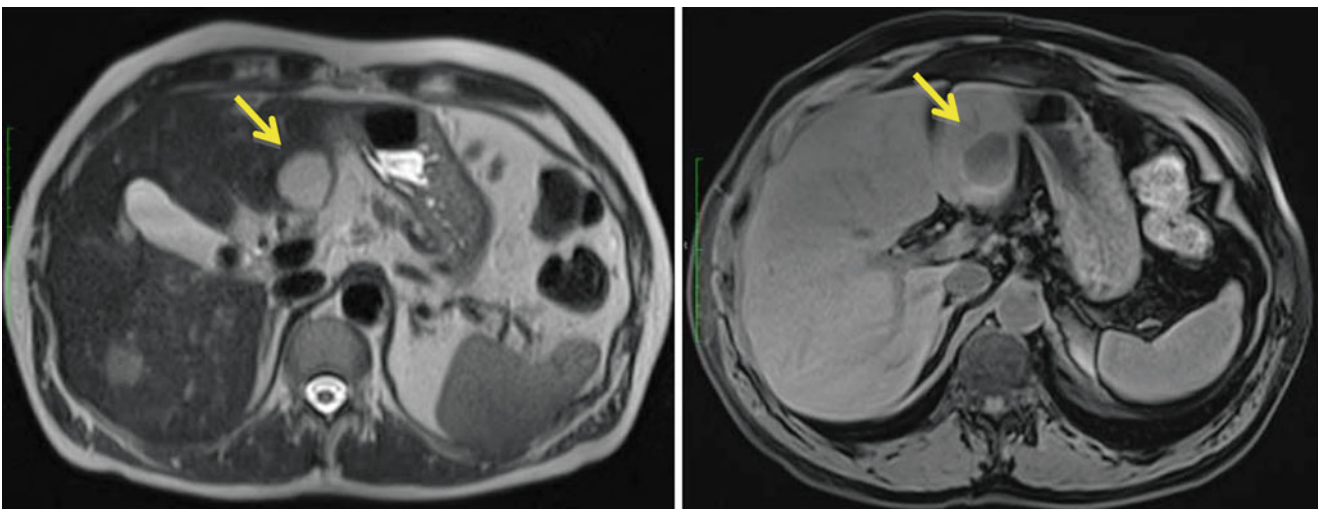


Fig. 10.17 Two different MR sequences of the liver T2 weighted HASTE (*left*) and T1 weighted eThrive (*right*) allowing to better characterize benign lesion (*arrow*) from metastatic lesions

Multi-Focal Lung Tumor

Clinical History

Seventy-year-old patient with history of smoking and incidental finding of a lung tumor on chest X-ray performed for investigation of resistant cough. Histology confirmed pulmonary carcinoma (cT2a cN3 cN0, stage IIB). Study requested for staging post chemotherapy.

Imaging Technique

PET: Whole-body PET acquired 60 min after injection of 370 MBq of ^{18}F -FDG.

MRI: Whole body atMR (T1 weighted), supine position. 3D FFE T1 weighted (eThrive) MRI followed by respiratory-gated T2 weighted HASTE images acquired in coronal and axial planes.

Findings

PET/MR shows a hypermetabolic lung lesion of the apical segment of the left lower pulmonary lobe. Identification of multiple metastatic lymph nodes with intense focal uptake of FDG in the paratracheal, hilar and subcarinal areas.

Teaching Points

While MR sequences are not optimal for examination of lung parenchyma that is best evaluated by CT, high resolution MR sequences can however provide sufficient anatomical details for identification and localization of lesions with high FDG uptake.

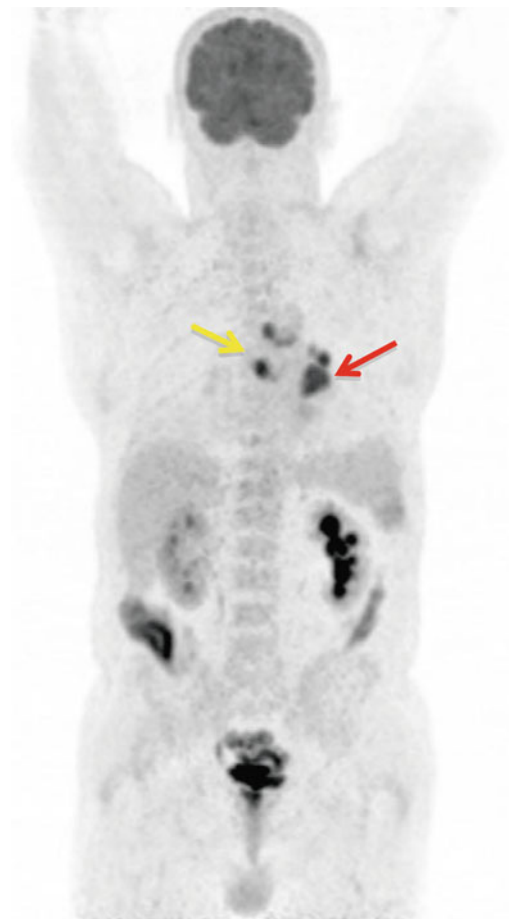


Fig. 10.18 Coronal view of volume rendered MIP images of PET showing the lung tumor of the lower left lobe (red arrow) and dissemination on the mediastinal lymph nodes (yellow arrow)

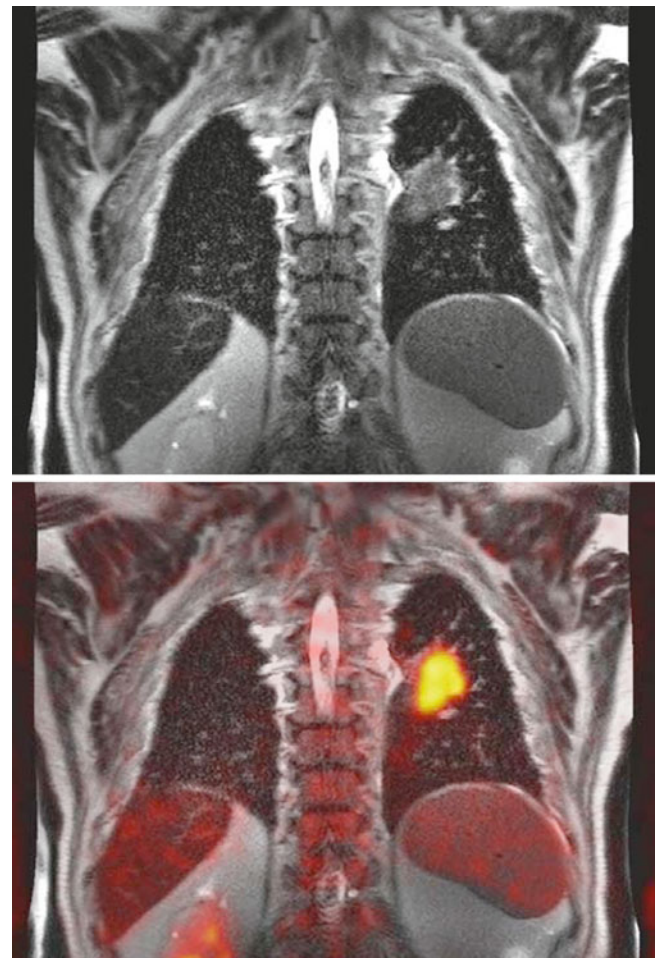


Fig. 10.19 Coronal respiratory-gated T2 weighted HASTE images (top) fused with corresponding PET image (bottom) showing high metabolic activity of the lung tumor

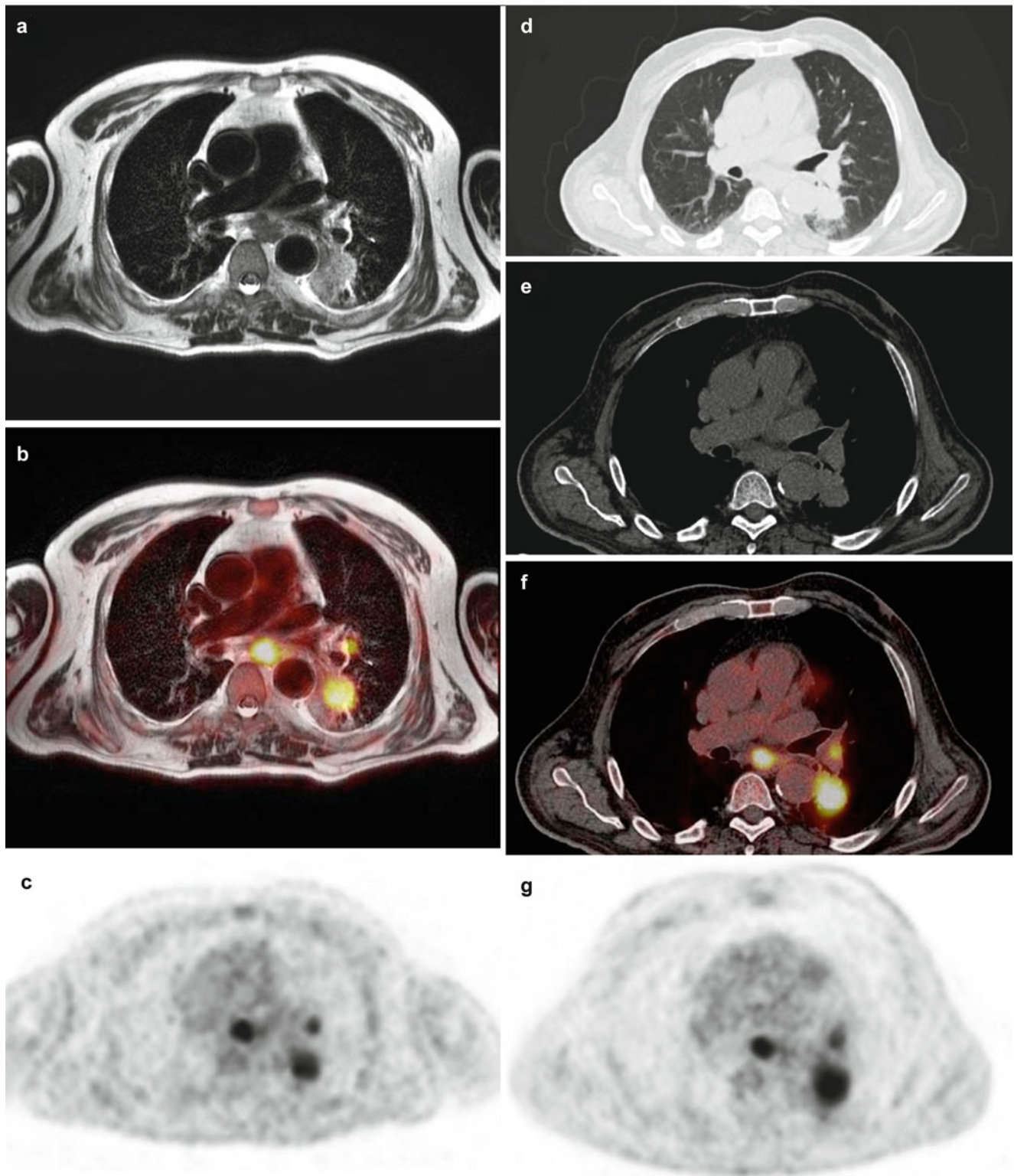


Fig. 10.20 Comparison of PET/MR (*left*) and PET/CT studies. Axial respiratory-gated T2 weighted HASTE images (**a**) fused with corresponding PET image (**b**), and axial CT with lung window setting (**d**)

and soft tissue setting (**e**) fused with corresponding PET images (**f**). Both (**c**) and (**g**) show the PET images at the same level of the two studies

Brain Metastasis of Unknown Origin

Clinical History

Sixty-two-year-old patient discovered having a brain metastases in the left cerebellum on an MRI performed for investigating recurrent headaches. Current study requested for staging and identification of the original tumor. Patient also known for renal insufficiency and multiple renal cysts.

Imaging Technique

PET: Whole-body PET acquired 60 min after injection of 369 MBq of ^{18}F -FDG, 57 kg/157 cm patient, with 5.2 mmol/L of fasting glycemia.

MRI: Whole body atMR (T1 weighted), supine position. 3D FFE T1 weighted (eThrive) MRI followed by a complete diagnostic MRI study of the abdomen.

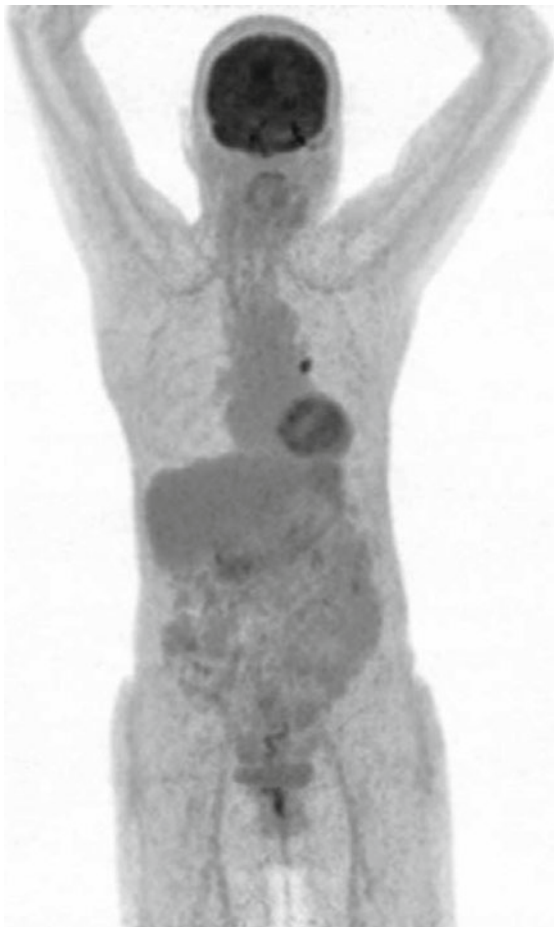


Fig. 10.21 Volume rendered MIP of whole-body PET showing a single focal uptake of a lesion in the hilar region of the left lung

Findings

PET/MR shows a focal hypermetabolic lesion of the hilum of the left lung. Standard whole-body MRI could not clearly characterize the lung lesion but complimentary PET/CT confirmed the suspicion of lung cancer. Additional high resolution MRI showed polycystic renal disease and incidental finding of an aortic dissection.

Teaching Points

For proper characterization of suspicious lung tumor, additional CT image are required. But PET/MR allows to properly stage the extent of remote metastatic lesions.

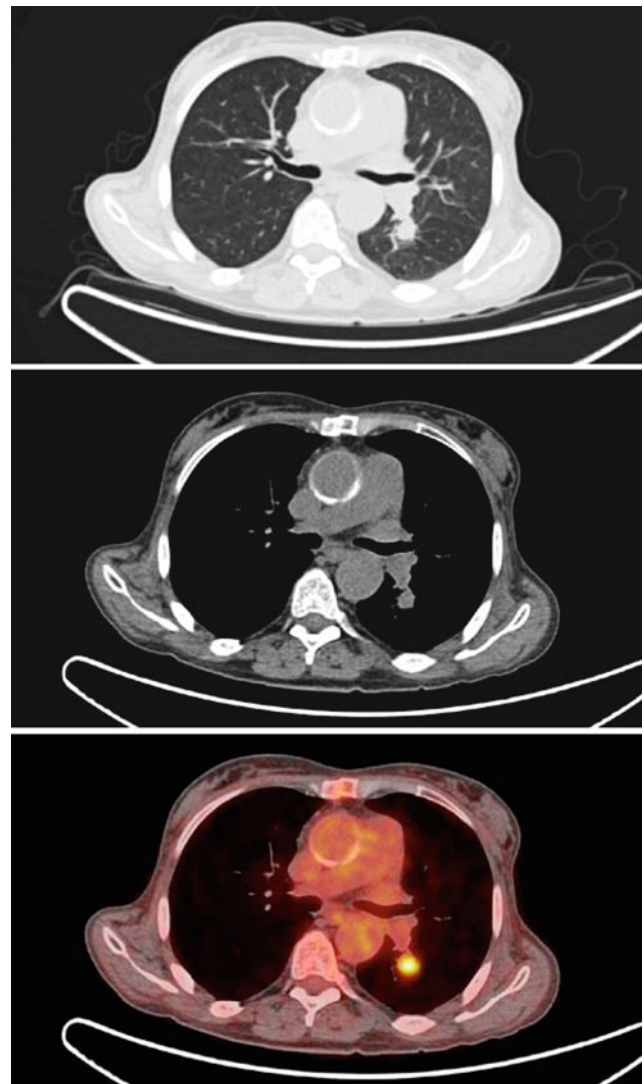


Fig. 10.22 Axial CT with lung window setting (*top*) and soft tissue setting (*middle*) fused with corresponding PET images (*bottom*)

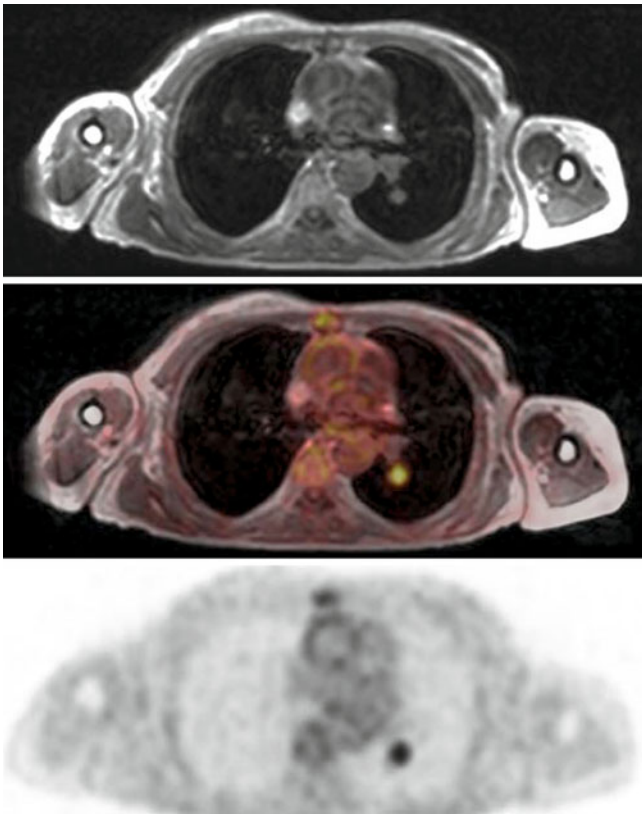


Fig. 10.23 Standard low-resolution whole body MRI sequences used for attenuation correction (*top*) have limited resolution for lung parenchyma

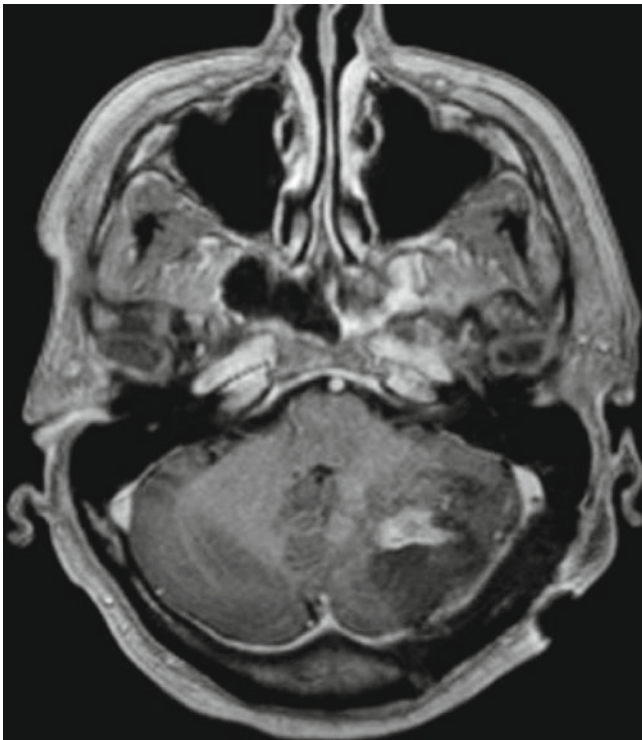


Fig. 10.24 Brain MRI post surgery showing the remaining extension of metastatic lesion of the left cerebellar region

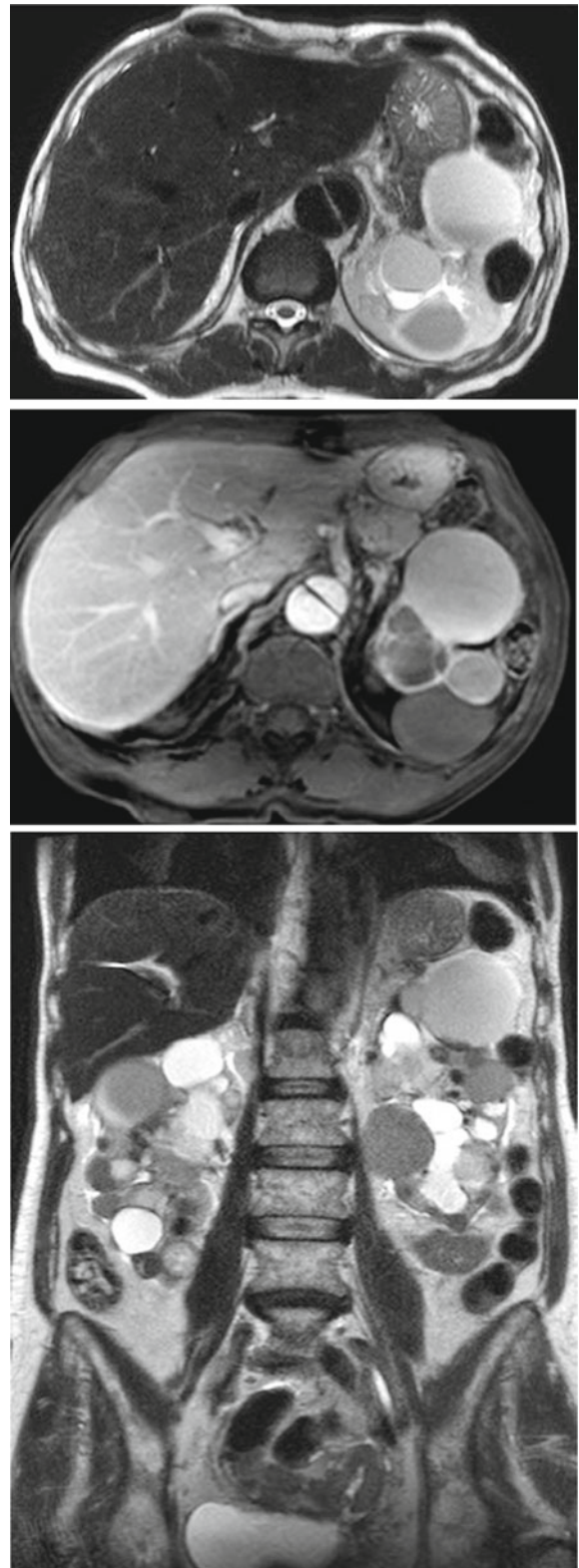


Fig. 10.25 Axial (*top*) and coronal (*bottom*) high resolution MR sequence of the abdomen show polycystic renal disease and incidental finding of an aortic dissection

Pulmonary Adenocarcinoma

Clinical History

Sixty-eight-year-old patient following incidental finding of a right lung mass on chest X-ray for chronic cough. CT guided biopsy confirmed a pulmonary adenocarcinoma. Study requested for staging and treatment planning.

Imaging Technique

PET: Whole-body PET acquired 60 min after injection of 370 MBq of ^{18}F -FDG.

MRI: Whole body atMR (T1 weighted), supine position. 3D FFE T1 weighted (eThrive) MRI followed by a whole body STIR acquisition.

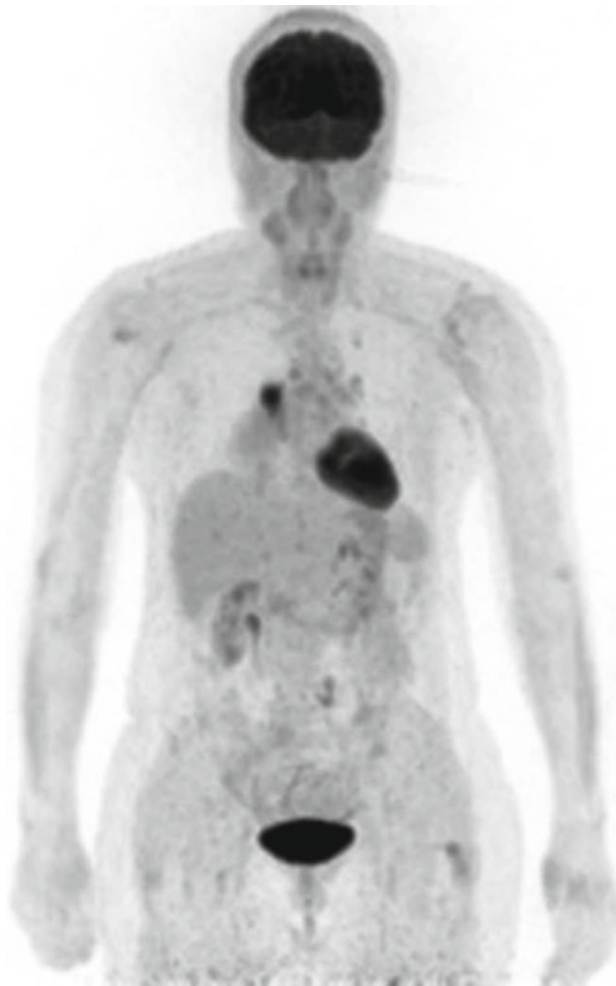


Fig. 10.26 Coronal projection of volume rendered MIP images of PET showing the hypermetabolic tumor lesion of the right lung with moderate FDG uptake of the surrounding pneumonia

Findings

PET/MR confirmed the presence of a hilar tumoral mass of the right lower lobe, associated with pneumonitis of the lower lobe secondary to partial obstruction of the bronchi by the tumor. Identification of multiple hypermetabolic lymph nodes of the mediastinum and subclavicular region

Teaching Points

PET images of PET/MR studies allow differentiating the extension of hypermetabolic tumor tissue from associated pneumonia with low or moderate FDG uptake.

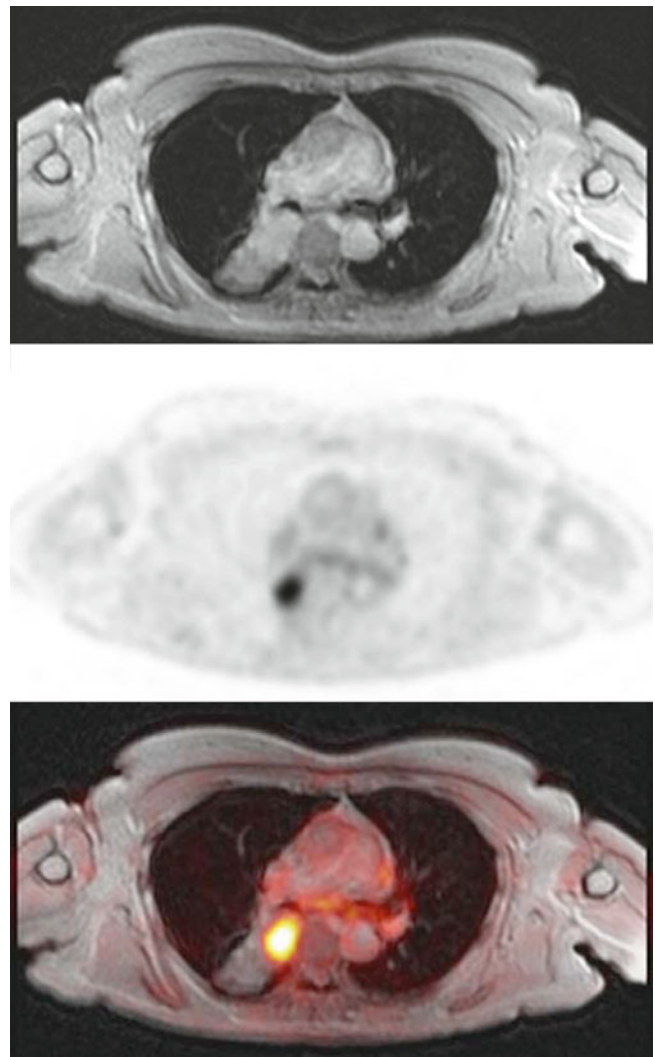


Fig. 10.27 Axial views from low resolution whole-body MR scan (*top*) and PET scan (*middle*) and fusion of the two images (*bottom*) showing the different FDG uptake between tumor and pneumonitis-induced condensation of pulmonary parenchyma

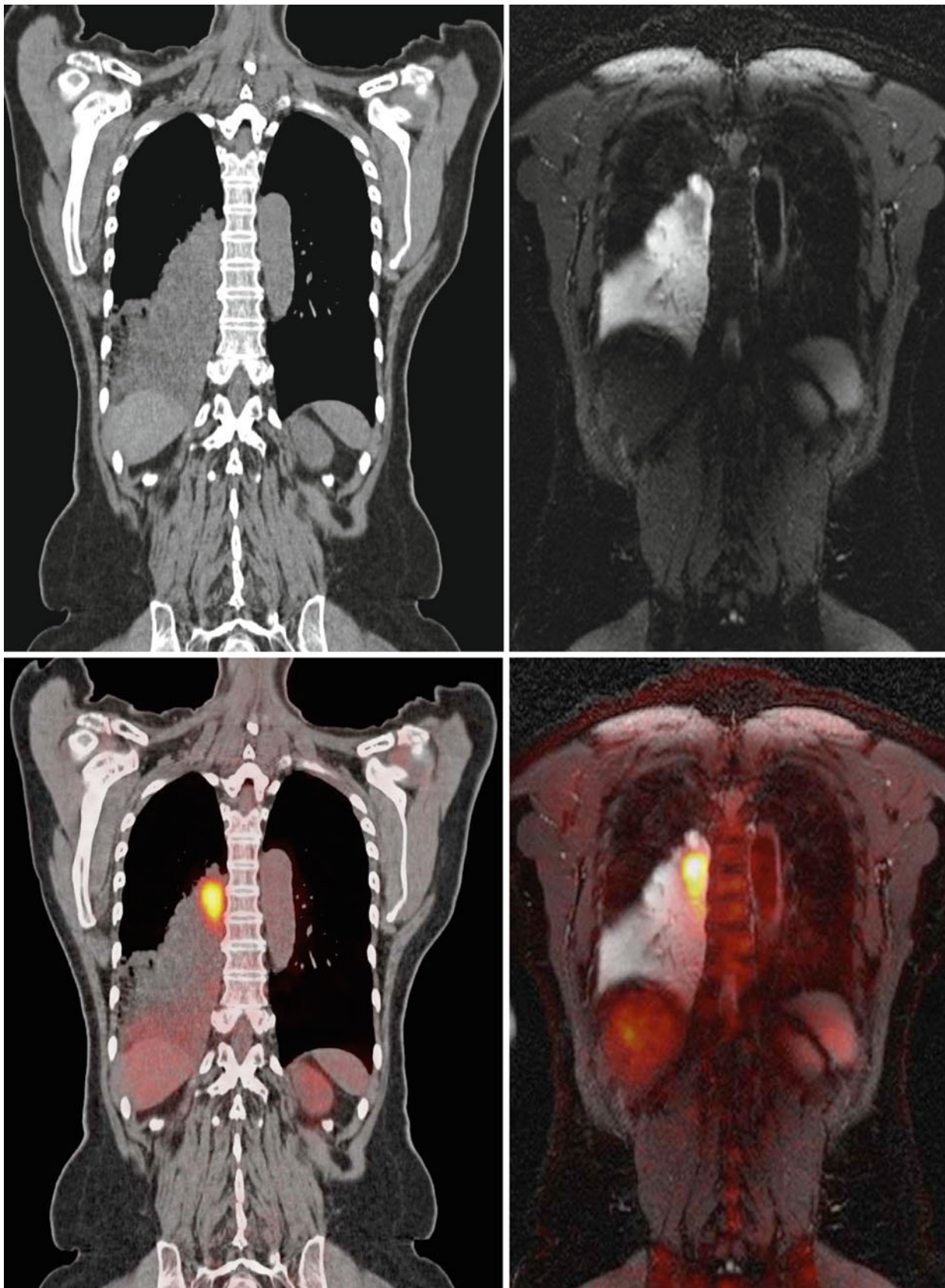


Fig. 10.28 Comparison of coronal reconstructed planes of PET/CT (*left*) and MRI STIR sequences (*right*) with fusion of corresponding PET images (*bottom*) showing the added value of PET for identifying hypermetabolic tumor tissue for the segmental pneumonitis

PET/MR in Acute Lymphocytic Leukemia (ALL)

Clinical History

A 44 year old patient with a pathological fracture of the lumbar spine previously stabilized with dorsal instrumentation. Histopathology revealed ALL-infiltration in the lumbar spine.

Imaging Technique

Whole body PET/MR images acquired 112 min after iv injection 408 MBq ^{18}F -FDG, 77 kg.

8 beds \times 5 min together with whole body cor T1w TSE and cor T2w STIR. Axial T1w VIBE fat saturated after Gadolinium over the region of the thorax, abdomen and pelvis.

Findings

A diffuse affection with bone marrow infiltration primarily of the lumbar and sacral spine is found in PET. MR demonstrates the extent of extra-osseous growth around the sacral bone.

Teaching Points

Combined PET/MR provides detailed information about the extent of the bone marrow infiltration. Smaller lesions might be missed by MR only but the high lesion-to-background ratio of PET facilitates their detection.

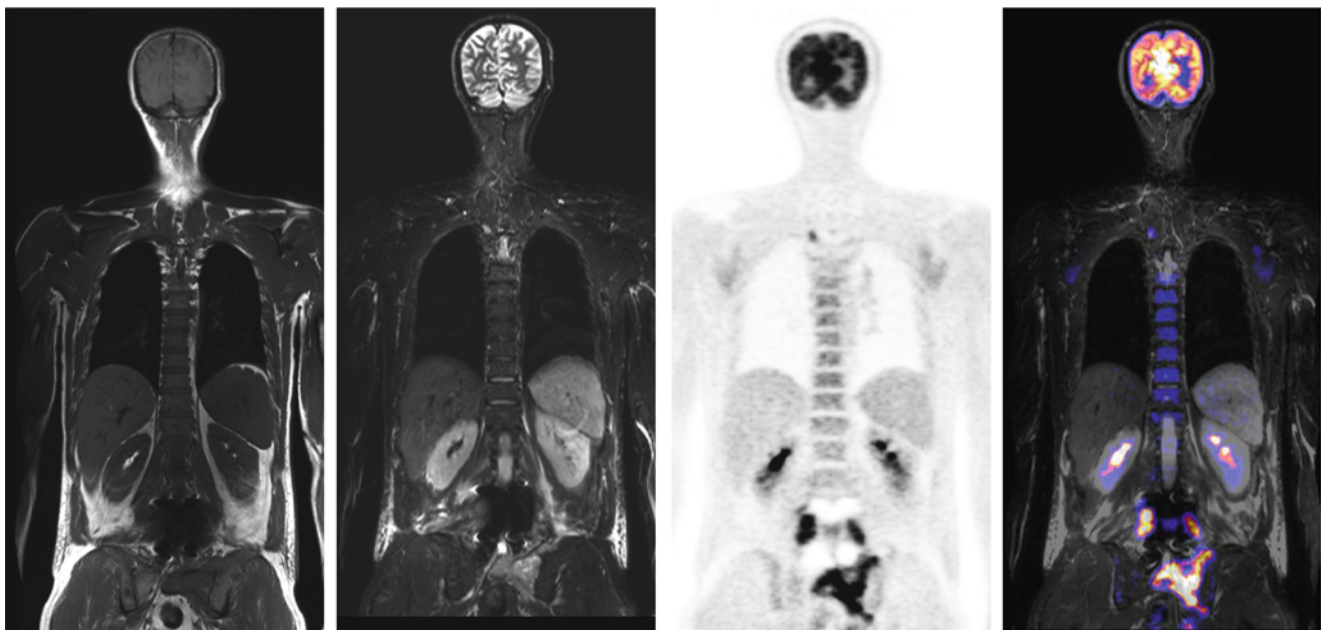


Fig. 10.29 Coronal T1w TSE (*far left*) and T2w STIR (*middle left*) show bone marrow infiltration in the left sacral bone, the left proximal femur, right ischium and the upper thoracic spine. Metal artifacts from the dorsal instrumentation obscure this region on MR images. PET

(*middle right*) and fused PET/MR (*far right*) images demonstrate high uptake of ^{18}F -FDG in the corresponding regions. The lesion in the upper thoracic spine might be missed on MR only, however the high lesion-to-background ratio on the PET images helps identifying it

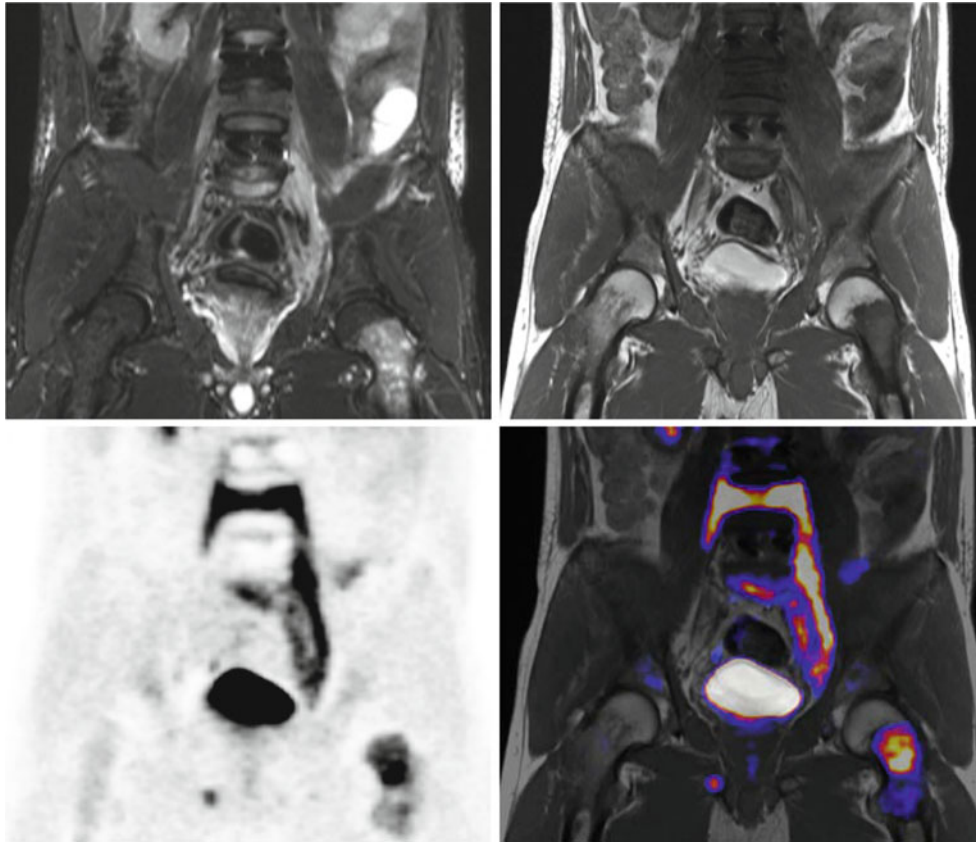


Fig. 10.30 Coronal T2w STIR and T1w TSE show a pathological fracture of L4 with artifacts from dorsal instrumentation in L3 and L5 (*upper row*). The T1w hypointense signal in L4 and the proximal left femur indicates complete infiltration of the vertebra by lymphoblastic cells. A small lesion is also found in the right pubic bone. In addition

T2w STIR demonstrates a hyperintense extraosseous strand on the left side reaching from L4 to the sacral bone. Another small extraosseous formation is present on the left side. Both PET and fused image confirm high uptake of ^{18}F -FDG in the corresponding regions (*lower row*)

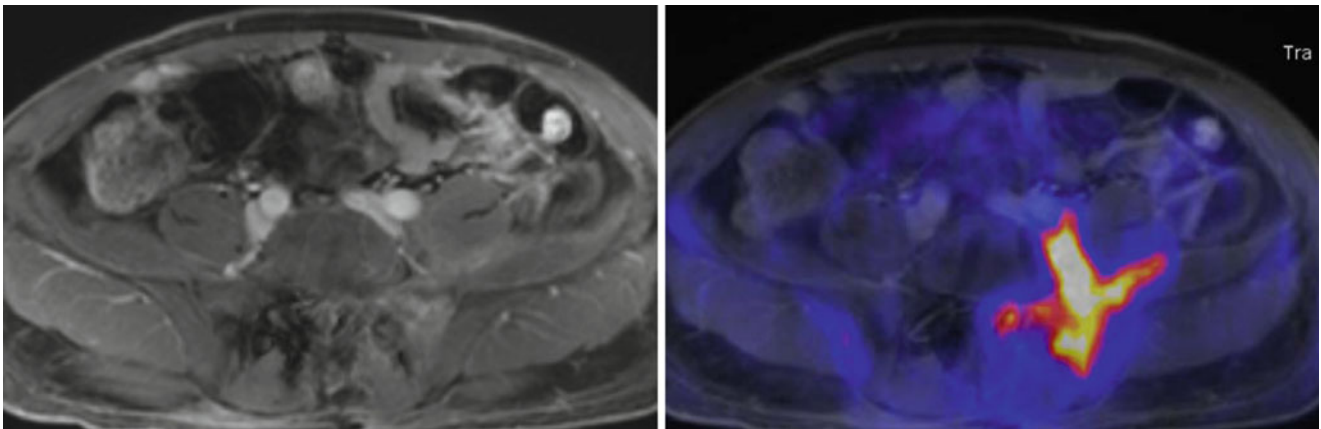


Fig. 10.31 The extraosseous tumor growth is better depicted in PET (*right*) compared to an axial T1w VIBE sequence (*left*) after Gadolinium with fat saturation. In this sequence only a diffuse low to moderate

contrast enhancement could be found, whereas the high lesion-to-background ratio in PET outlines the spread more clearly

PET/MR for Biopsy Planning in NHL with Bone Infiltration

Clinical History

A 54 year old patient presents chronically elevated leucocytes and the suspicion of lymphoma. No suspicious lymph nodes were found on CT.

Imaging Technique

Whole body PET/MR images acquired 174 min after iv injection 444 MBq 18F-FDG, 95 kg.

4 beds \times 4 min together with whole body cor T1w TSE and axial T2w HASTE fs. 1 bed (pelvis) a 4 min together with cor T2w STIR and axial T1w fs after Gadolinium.

Findings

T1w TSE and T2w STIR show a patchy bone marrow infiltration with islands of normal bone interposed between. Note the extensive artifacts from a hip prosthesis on the left side especially impairing the fat suppression.

Teaching Points

The combination of whole-body PET and MR can aid in guiding biopsy in patients with lymphoma especially in atypical cases like primary bone infiltration. The information of T1w TSE and T2w STIR delineate areas of bone infiltration against the normal bone marrow. In contrast, CT often shows no pathological finding.

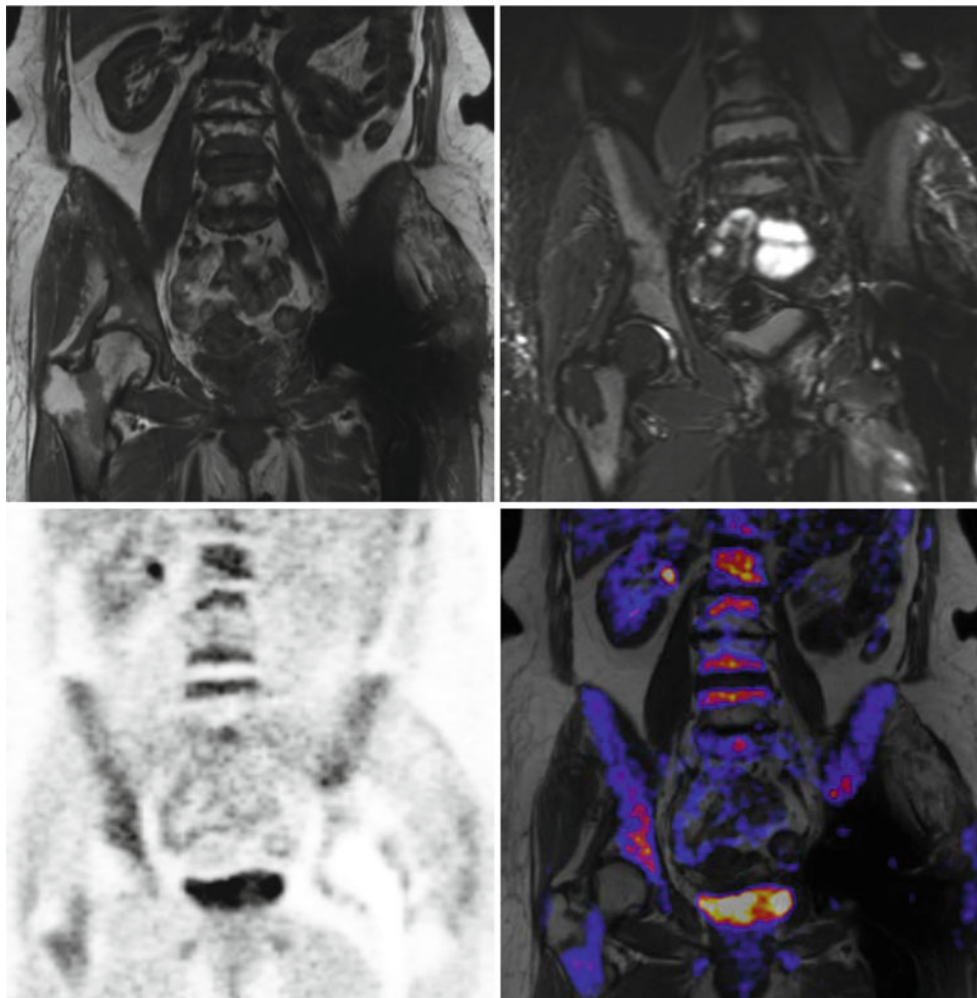


Fig. 10.32 Coronal T1w TSE and T2w STIR show patchy bone marrow infiltration of the lumbar spine and pelvis (*upper row*). Note the normal interposed bone marrow between the affected areas. Coronal

PET shows moderate increase tracer uptake in the lumbar spine and pelvis. Fused PET and T1w TSE demonstrate good correlation between the uptake in PET and the hypointense regions in T1w (*lower row*)

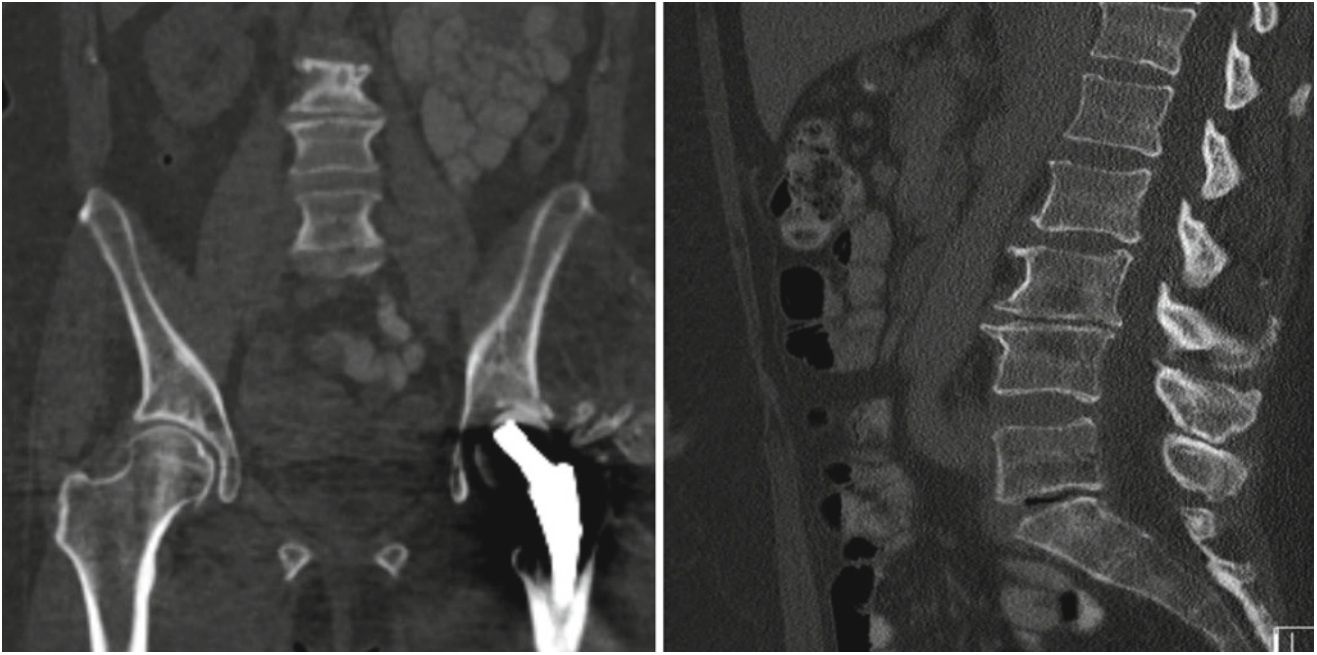


Fig. 10.33 In the coronal (*left*) and sagittal (*right*) reformatted bone window from CT no abnormalities could be detected underlining the value of bone marrow imaging in MRI

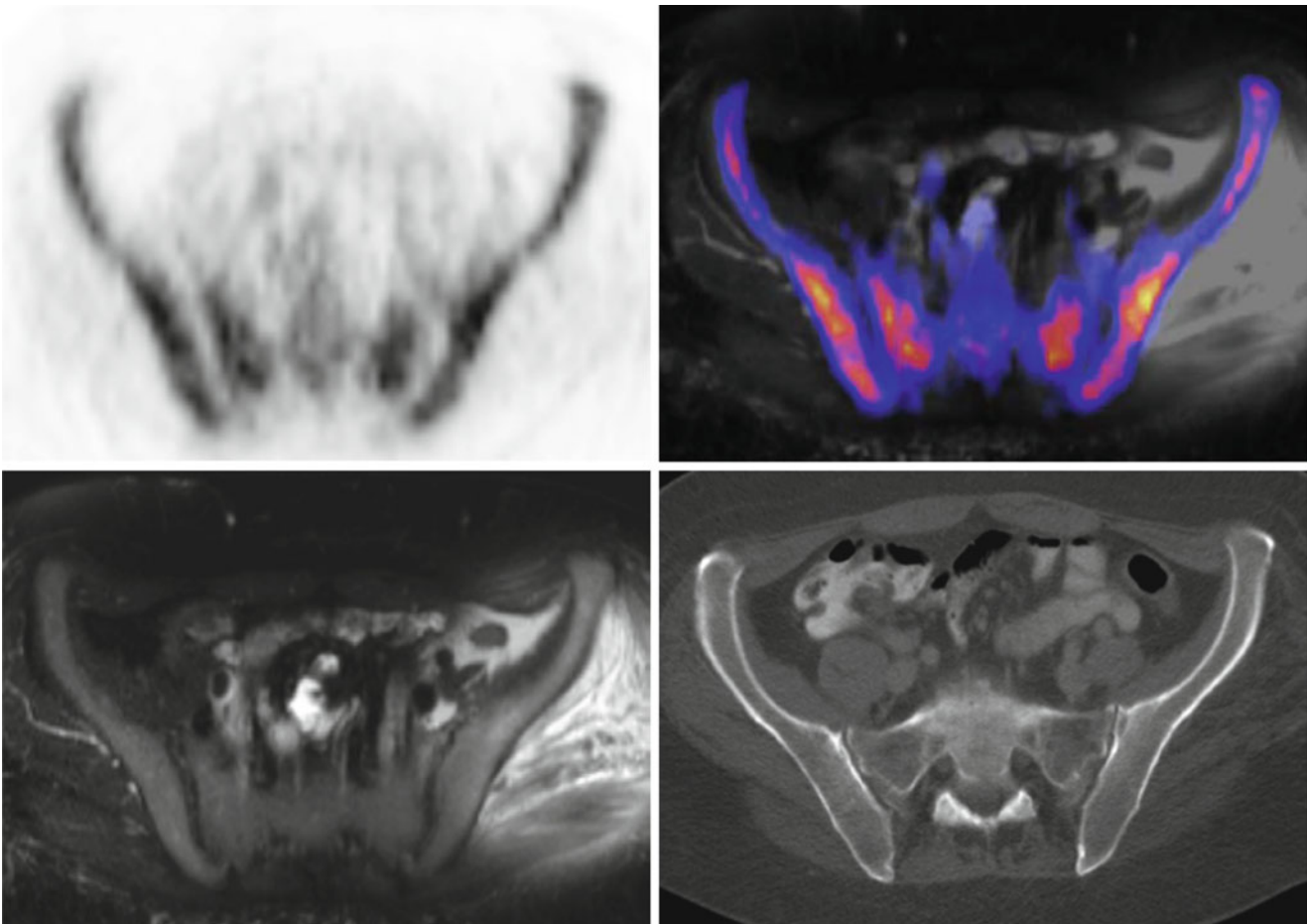


Fig. 10.34 Axial PET and fused images show a patchy infiltration of the pelvis and sacral bone (*upper row*). Diffuse hyperintensity in T2w HASTE fs in MRI demonstrate the replacement of fatty marrow in the

corresponding region (*left, lower row*). In CT no abnormalities could be detected (*right, lower row*). Incomplete fat suppression is related to hip prosthesis on the left side

Recurrent T-NHL with Bone Infiltration

Clinical History

A 60 year old patient with prior T-NHL presents with pain in the right hip. CT demonstrates diffuse osteolyses in the right acetabulum raising the suspicion of a recurrence with bone infiltration.

Imaging Technique

Whole body PET/MR images acquired 117 min after iv injection 367 MBq 18F-FDG, 78 kg.

4 beds \times 5 min together with whole body coronal T1w TSE and cor T2w STIR. Whole body axial T1w flash fat saturated after Gadolinium.

Findings

In contrast to CT T1w TSE clearly outlines the area of bone infiltration by recurrent NHL. It corresponds to an intense high uptake of 18F-FDG.

Teaching Points

The combination of PET and MRI can demonstrate the extent of bone marrow infiltration more clearly than PET/CT. Especially T1w TSE sequences outline the replacement of fatty bone marrow by malignant tissue better than CT.

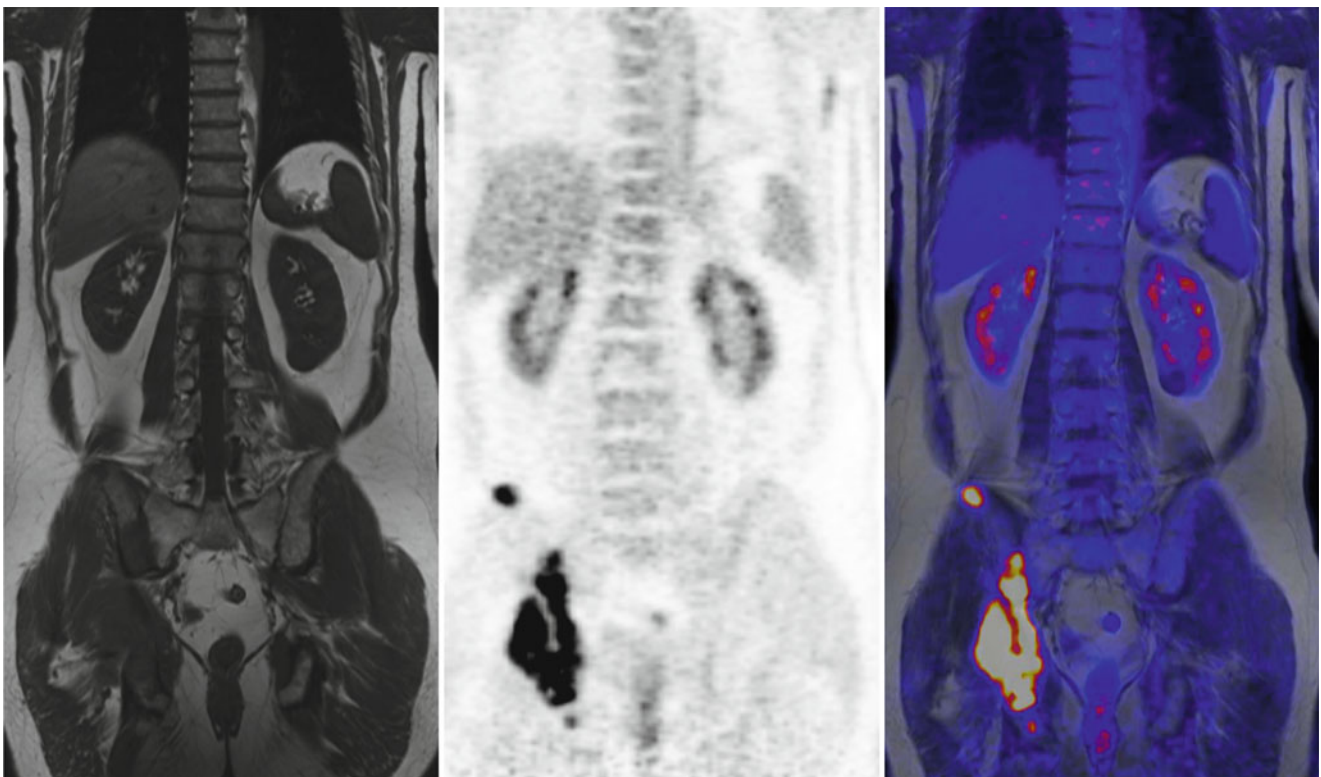


Fig. 10.35 Coronal T1w TSE (*left*) show a nodular hypointensity in the iliac crest on the right side and a diffuse bone marrow infiltration of the right acetabulum. Coronal PET demonstrate high focal uptake in the

corresponding regions (*middle*). A good correlation between the findings in MR and PET is outlined in the fused dataset (*right*)

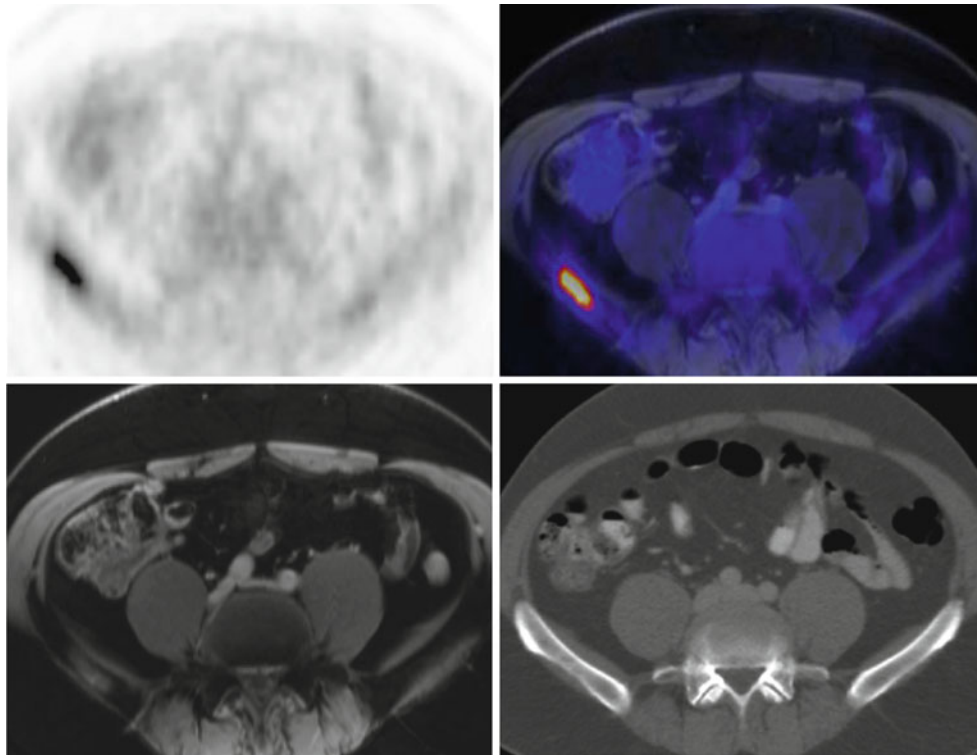


Fig. 10.36 Axial PET and fused PET images show a high uptake in the right pelvis (*upper row*). Intense contrast enhancement is found in the fat saturated T1w sequence after Gadolinium (*lower row, left*). The

corresponding CT exhibits a faint sclerosis in the corresponding region (*lower row, right*)

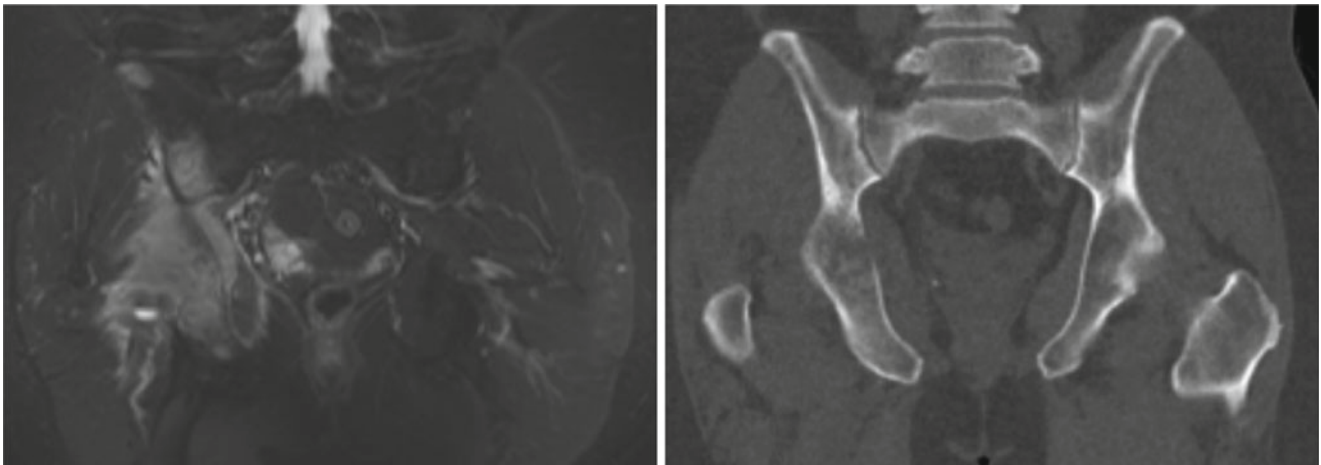


Fig. 10.37 A direct comparison of T2w STIR (*left*) and CT (*right*) demonstrates the superiority of MR in outlining the infiltration of bone marrow. In the CT lesions in the iliac crest and near the ileo-sacral joint cannot be visualized

Liver Metastasis of Adenocarcinoma of the Adrenal Gland

Clinical History

Thirty-five-year-old patient with adenocarcinoma of the left adrenal gland undergoing a staging examination.

Imaging Technique

Whole body PET/MR images acquired 46 min after iv injection of 359 MBq 18F-FDG, 67 kg.

4 beds \times 4 min together with coronal T1w TSE and axial T2w haste fs. 1 bed (upper abdomen) a 15 min together with ax/cor T2 HASTE, ax EPI (DWI), ax T1-VIBE dynamic post i.v. Gd.

Findings

In the right liver lobe a large focal lesion that is hyperintense on T2-weighted sequence can be depicted. The lesion shows a hyperintense signal in diffusion-weighted imaging both at a low and a high b -value suggesting a restricted diffusion within a likely hypercellular lesion. There is intense focal uptake of 18F-FDG in PET. Both MRI and PET strongly indicate a liver metastasis.

Teaching Points

Diffusion-weighted MR imaging (DWI) is an important MR sequence for both detection and characterization of focal liver lesions. In malignant lesions often a restricted diffusion due to hypercellularity can be seen.

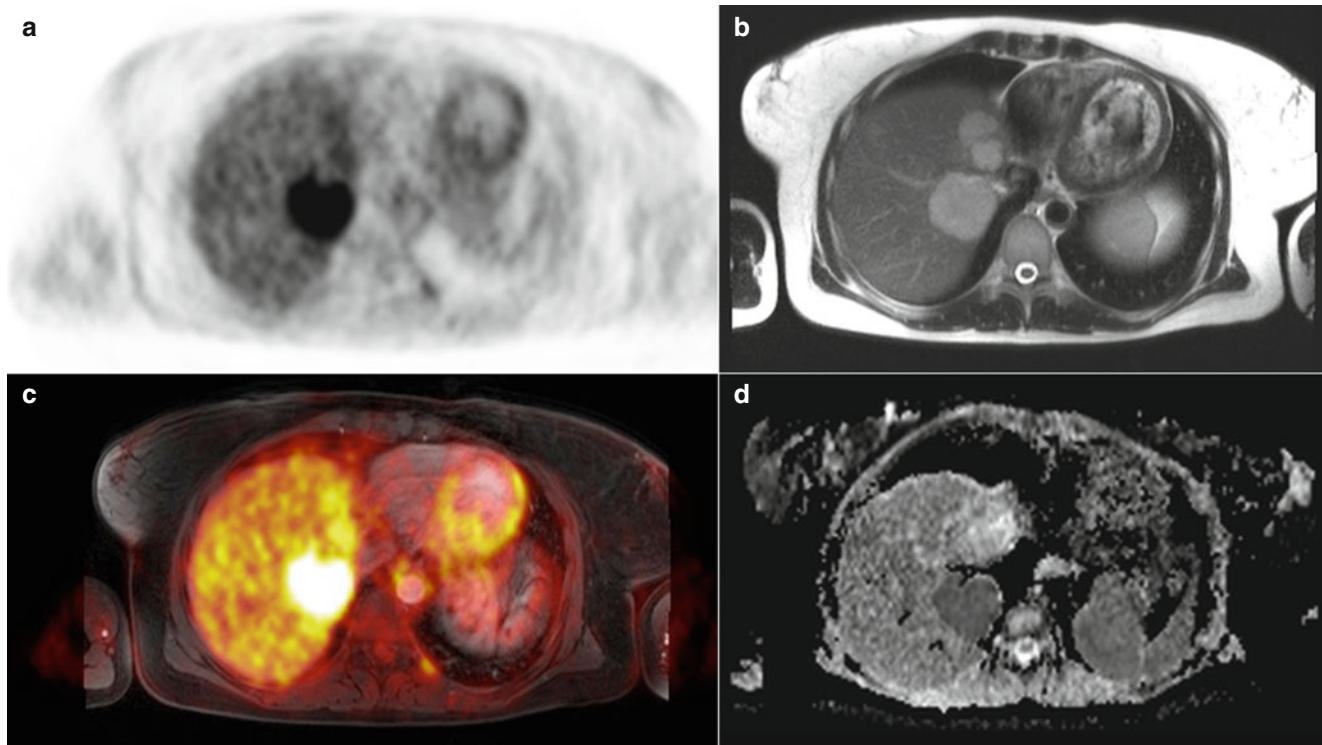


Fig. 10.38 In the right liver lobe a large focal lesion with intense focal uptake of 18F-FDG is seen (a). The lesion is hyperintense in a T2-weighted sequence (b). A low ADC-value (d) suggests a hypercellular lesions. Both MRI and PET indicate one vital and one avital liver metastasis (c and d)

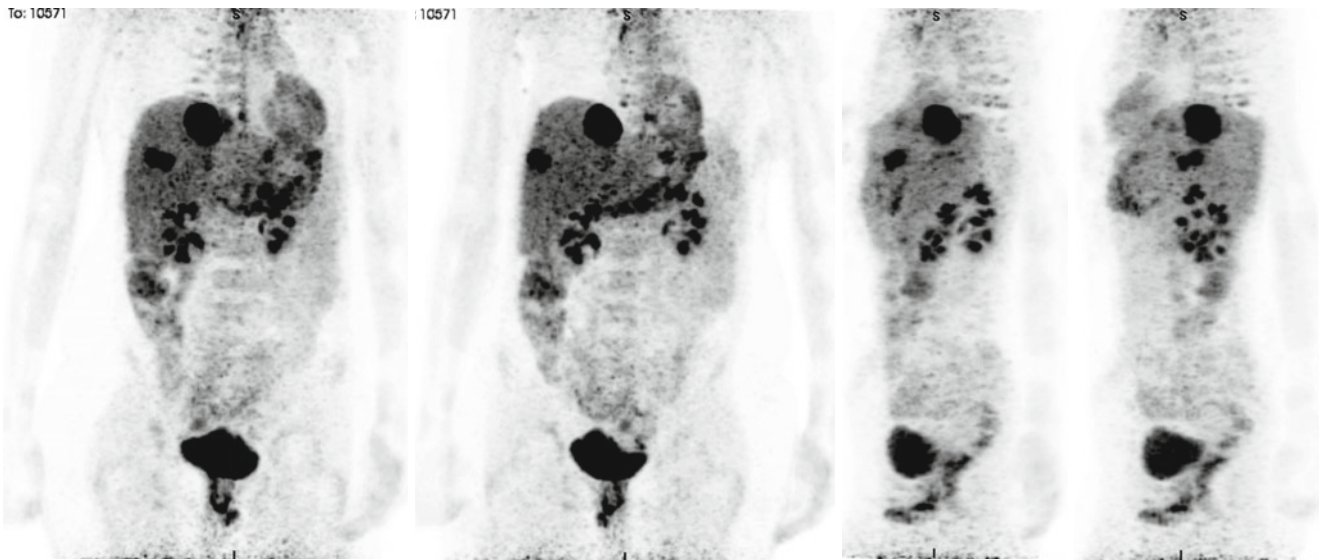


Fig. 10.39 Whole-body ^{18}F -FDG-PET in the coronal plane. Except for the liver there is no evidence for metastases to other organs

Liver Metastases of Colorectal Cancer

Clinical History

Sixty-one-year-old patient with known liver metastases of colorectal cancer and a history of partial liver resection and radiofrequency ablation.

Imaging Technique

Whole body PET/MR images acquired 46 min after iv injection of 357 MBq ^{18}F -FDG, 73 kg.

4 beds \times 4 min together with coronal T1w TSE and axial T2w HASTE fs. 1 bed (upper abdomen) a 15 min together with ax/cor T2 HASTE, ax EPI (DWI), ax T1-VIBE dynamic post i.v. Gd.

Findings

Adjacent to the ablation defect in the left liver lobe a circular enhancement can be seen in the arterial phase after i.v. administration of contrast material. Another area of focal enhancement is seen in the right liver lobe. Both regions show an intense uptake of ^{18}F -FDG in PET and are highly suspicious of newly developed liver metastases.

Teaching Points

Dynamic contrast-enhanced MR imaging together with PET is a valuable tool in the detection of liver metastases, especially in patients with previous treatment either by surgery or focal ablative techniques like radiofrequency ablation.

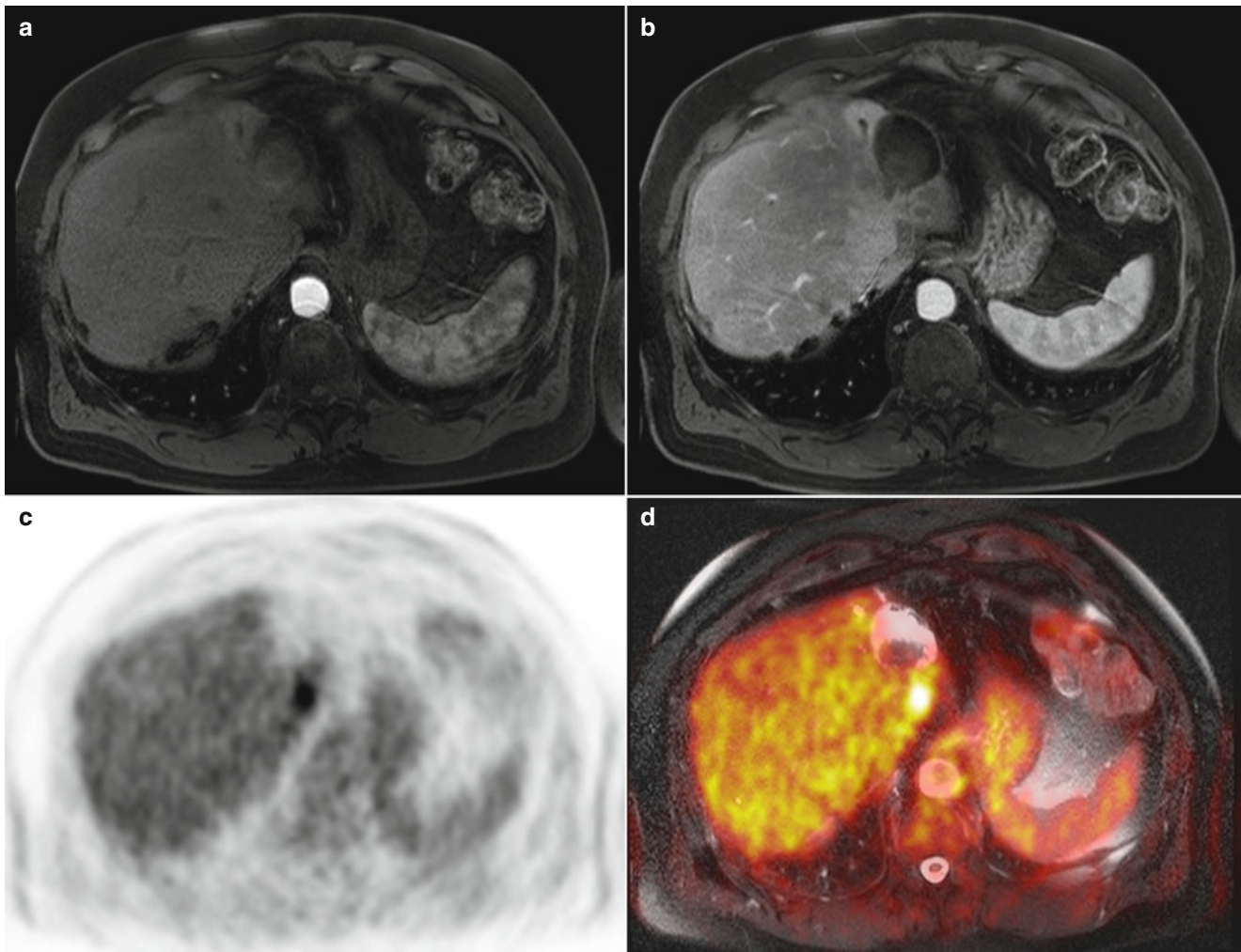


Fig. 10.40 Adjacent to the ablation defect in the left liver lobe a circular enhancement can faintly be seen in the early and late arterial phase after i.v. administration of contrast material (a and b). PET (c) and fusion (d) nicely delineate the area of recurrence

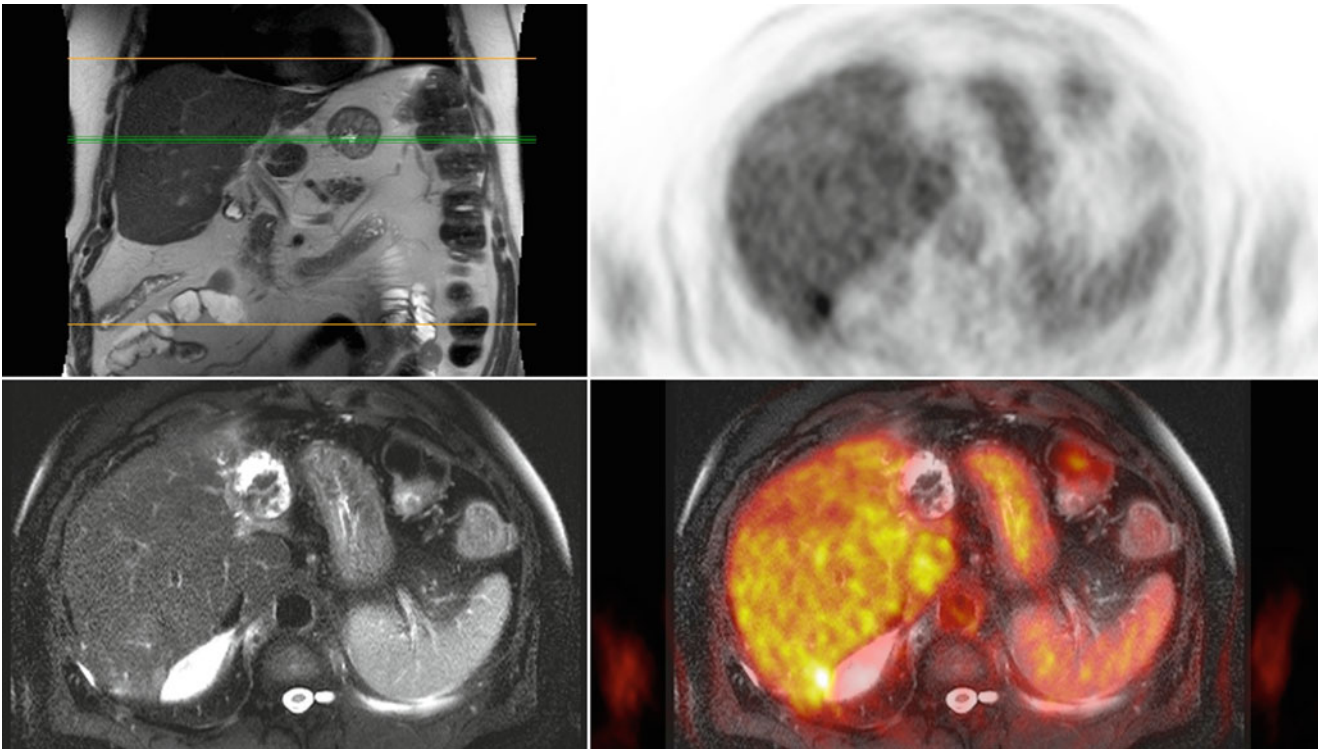


Fig. 10.41 Another PET positive lesion in the right lobe shows an faint T2w hyperintensity

Liver Metastasis of Rectal Cancer

Clinical History

Forty-six-year-old patient with rectal cancer undergoing a staging examination.

Imaging Technique

Whole body PET/MR images acquired 46 min after iv injection of 487 MBq ^{18}F -FDG, 100 kg.

4 beds \times 4 min together with coronal T1w TSE and axial T2w haste fs. 1 bed (upper abdomen) a 15 min together with ax/cor T2 HASTE, ax EPI (DWI), ax T1-VIBE dynamic post i.v. Gd.

Findings

In the left liver lobe a focal lesion with restricted diffusion and peripheral enhancement is seen. There is intense focal uptake of ^{18}F -FDG in PET. Both MRI and PET strongly indicate a liver metastasis. No additional focal lesions are seen.

Teaching Points

In patients with colorectal cancer accurate staging of liver metastases is of paramount importance as patients eligible for resection of metastases can be treated curatively. Combination of a dedicated MR protocol of the liver and ^{18}F -FDG PET imaging is helpful regarding the detection of liver metastases.

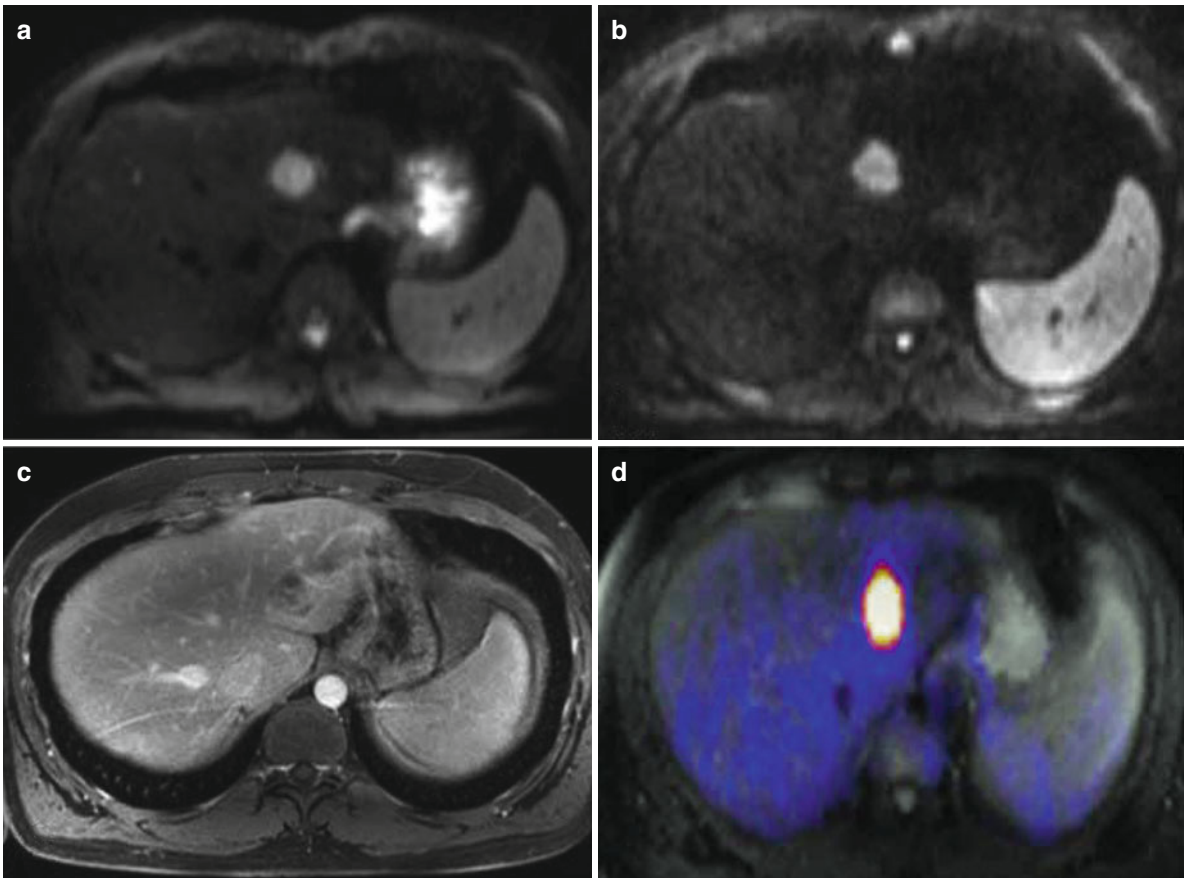


Fig. 10.42 In the left liver lobe a focal liver lesion is seen. It is hyperintense in DWI on both low (a) and high (b) *b*-value images reflecting restricted diffusion. In the portal venous phase the lesion shows peripheral

enhancement (c). In addition intense focal uptake of ^{18}F -FDG is seen (d). Both MRI and PET strongly indicate a liver metastasis

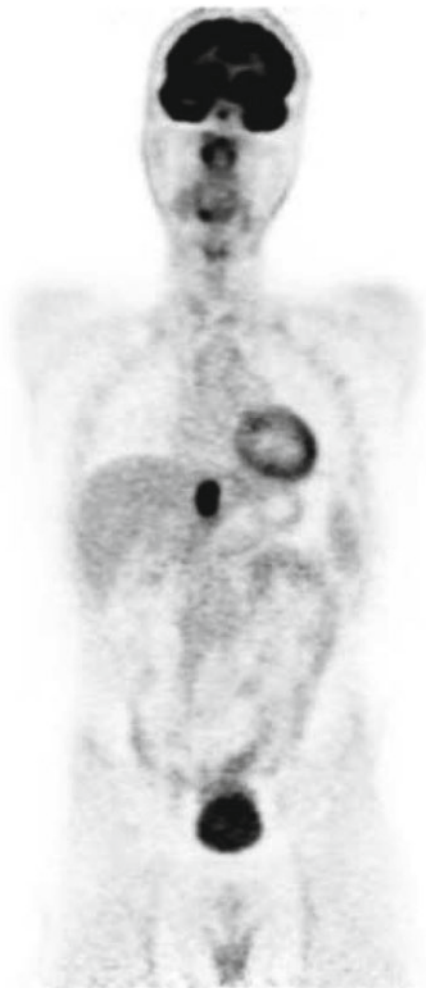


Fig. 10.43 Whole-body ^{18}F -FDG-PET in the coronal plane. Except for the liver there is no evidence for metastases to other organs

References

1. Hutchings M, Barrington SF (2009) PET/CT for therapy response assessment in lymphoma. *J Nucl Med* 50(Suppl_1):21S–30S
2. Kwee TC, Van Ufford HMEQ, Beek FJ, Takahara T, Uiterwaal CS, Bierings MB et al (2009) Whole-body MRI, including diffusion-weighted imaging, for the initial staging of malignant lymphoma: comparison to computed tomography. *Invest Radiol* 44(10):683–690
3. Punwani S, Taylor SA, Bainbridge A, Prakash V, Bandula S, Vita ED et al (2010) Pediatric and adolescent lymphoma: comparison of whole-body STIR half-Fourier RARE MR imaging with an enhanced PET/CT reference for initial staging. *Radiology* 255(1):182–190
4. Lin C, Luciani A, Itti E, El-Gnaoui T, Vignaud A, Beaussart P et al (2010) Whole-body diffusion-weighted magnetic resonance imaging with apparent diffusion coefficient mapping for staging patients with diffuse large B-cell lymphoma. *Eur Radiol* 20(8):2027–2038
5. Wu L-M, Chen F-Y, Jiang X-X, Gu H-Y, Yin Y, Xu J-R (2012) 18F-FDG PET, combined FDG-PET/CT and MRI for evaluation of bone marrow infiltration in staging of lymphoma: a systematic review and meta-analysis. *Eur J Radiol* 81(2):303–311
6. Abdulqadhr G, Molin D, Aström G, Suurküla M, Johansson L, Hagberg H et al (2011) Whole-body diffusion-weighted imaging compared with FDG-PET/CT in staging of lymphoma patients. *Acta Radiol* 52(2):173–180
7. Antoch G, Vogt FM, Freudenberg LS, Nazaradeh F, Goehde SC, Barkhausen J et al (2003) Whole-body dual-modality PET/CT and whole-body MRI for tumor staging in oncology. *JAMA* 290(24):3199–3206
8. Schmidt GP, Baur-Melnyk A, Herzog P, Schmid R, Tiling R, Schmidt M et al (2005) High-resolution whole-body magnetic resonance image tumor staging with the use of parallel imaging versus dual-modality positron emission tomography-computed tomography: experience on a 32-channel system. *Invest Radiol* 40(12):743–753
9. Liu J, Yang X, Li F, Wang X, Jiang X (2011) Preliminary study of whole-body diffusion-weighted imaging in detecting pulmonary metastatic lesions from clear cell renal cell carcinoma: comparison with CT. *Acta Radiol* 52(9):954–963
10. Lauenstein TC, Goehde SC, Herborn CU, Goyen M, Oberhoff C, Debatin JF et al (2004) Whole-body MR imaging: evaluation of patients for metastases. *Radiology* 233(1):139–148
11. Schwenzer NF, Schraml C, Müller M, Brendle C, Sauter A, Spengler W et al (2012) Pulmonary lesion assessment: comparison of whole-body hybrid MR/PET and PET/CT imaging—pilot study. *Radiology* 264(2):551–558